Does More Moisture in the Atmosphere Lead to More Intense Rains?

Jun–ichi Yano, Jun-Ichi Yano, Agostino Manzato

Does More Moisture in the Atmosphere Lead to More Intense Rains?

JUN-ICHI YANO[a] AND AGOSTINO MANZATO[b]

[a] *CNRM, UMR 3589 (CNRS), Météo-France, Toulouse, France*
[b] *ARPA Friuli Venezia Giulia–OSMER, Palmanova (UD), Italy*

(Manuscript received 5 May 2021, in final form 8 November 2021)

ABSTRACT: It is typically interpreted that more moisture in the atmosphere leads to more intense rains. This notion may be supported, for example, by taking a scatterplot between rain and column precipitable water. The present paper suggests, however, that the main consequence of intense rains with more moisture in the atmosphere is that there is a higher chance of occurrence rather than an increase in the expected magnitude. This tendency equally applies to any rains above 1 mm $(6\ h)^{-1}$ to a lesser extent. The result is derived from an analysis of 33 local rain gauge station data and a shared sounding over Friuli Venezia Giulia, northeast Italy.

SIGNIFICANCE STATEMENT: Moisture is the source of clouds. Clouds, in turn, are source of rain. So we may expect that more moisture in the atmosphere causes more intense rains. We may further speculate that with more moisture in the atmosphere as a consequence of the global warning, we must face more catastrophic rain events and floods. However, this paper, by analyzing data over Friuli Venezia Giulia, northeast Italy, suggests otherwise: more moisture indeed increases frequencies of intense rains, but not their magnitudes as much.

KEYWORDS: Atmosphere; Europe; Atmospheric circulation; Atmospheric river; Convection; Extreme events; Precipitation; Rainfall; Hydrologic cycle

1. Introduction

Rain[1] is produced from moisture of the atmosphere: clouds are first formed by condensation of water vapor, then cloud water transforms into rain (cf. Dingman 1994). For this reason, it is a popular belief that high moisture in the atmosphere is a crucial prerequisite for significant rains. Observed association of extreme rains with high moisture (e.g., Khodayar et al. 2018; Grazzini et al. 2020) supports this belief. As a result, the question of rain formation, to be studied by itself (Pruppacher and Klett 1997; Khain and Pinsky 2018), is often reduced to that of tracing a moisture source (e.g., Trenberth 1998; Sorí et al. 2019).

This line of investigation leads to a picture that bulk of moisture in midlatitudes is transported from the tropics through narrow moisture ducts, called "atmospheric rivers" (Zhu and Newell 1994), that *cause* extreme rains and floods (e.g., Lavers et al. 2011; Lavers and Villarini 2013; Ralph et al. 2013; Waliser and Guan 2017). A more specific link between extreme rains over Italy and atmospheric rivers is suggested by case studies of Bertó et al. (2004), De Zolt et al. (2006), Malguzzi et al. (2006), and Buzzi et al. (2014). Krichak et al. (2004, 2006, 2015) even argue that moisture causing extreme rains at midlatitudes, including those over Italy, are traced back to tropical cyclones about a week earlier.

However, does tracing a moisture source, especially over a great distance, explain all about extreme rains and floods? With this ultimate, fundamental question in mind, the present paper investigates the relationship between the available moisture in the atmosphere and the rain intensity. We emphasize the importance of distinguishing between the *frequency* (or the chance) and the *intensity* of rain. Two quantities are clearly linked together. However, one does not necessarily follow from another. More precisely, the present paper is going to suggest that although the rain frequency increases with increasing moisture in the atmosphere, an increase of rain intensity does not necessarily follow.

For this investigation, the study adopts combination of sounding-derived data and rain gauge measurements over the Friuli Venezia Giulia (FVG) Plain, northeast Italy, as detailed in the next section. Here, a sounding balloon measures the moisture as it ascends over the troposphere, typically traversing over a distance on the order of 10^2 km. This scale roughly corresponds to that of the FVG Plain. On the other hand, a rain gauge measures the rain strictly locally. By combining these two sets of data, the study examines the statistical characteristics of local rain under a given background state of moisture in the atmosphere: as the moisture increases as a background state, is it the "chance of rain" or the "expected rain intensity" that increases at individual

[1] The term, rain, is adopted throughout the paper rather than a more formal term, precipitation, but by including all possible rain forms (snow, hail, etc), for a better general readability of the text.

Denotes content that is immediately available upon publication as open access.

Supplemental information related to this paper is available at the Journals Online website: https://doi.org/10.1175/JAS-D-21-0117.s1.

Corresponding author: Jun-Ichi Yano, jun-ichi.yano@cnrs.fr

DOI: 10.1175/JAS-D-21-0117.1

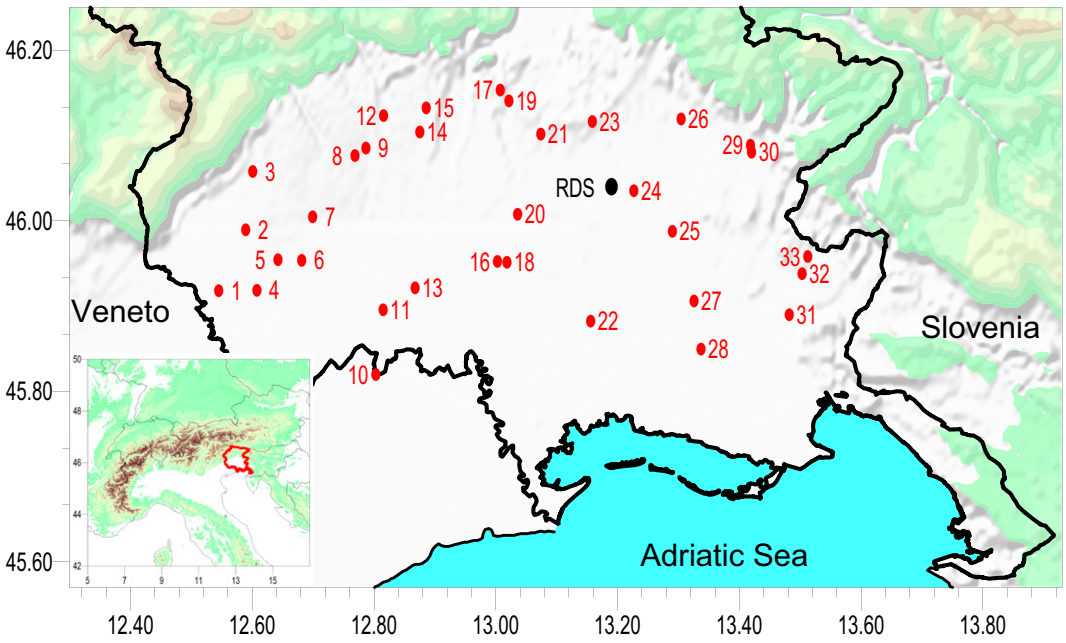

FIG. 1. Map of the Friuli Venezia Giulia (FVG) Plain. Location of the Udine-Campoformido radiosounding (managed by the Italian Areonautica Militare), used for evaluating CPW, is marked as RDS in black. Locations of the 33 rain gauge stations (managed by the FVG Civil Protection) used in the analysis are marked in red by the numbers that correspond to those in Table 1.

points of the surface? After further discussion, this question is presented in a more formal manner in section 3e.

The purpose of the present paper is to address this question by adopting data from a single region as just described. The results obtained are tentative at best, although the authors expect its generality, as argued in the final discussion section. Rather, the main contribution of the present paper is to propose a solid methodology to address this question objectively based on a probabilistic formulation (section 3), and to provide a demonstrative case. The present work adds a new thread to already-existing extensive applications of the probability theories to the rain (e.g., Besson 1924; Epstein 1966; Jorgensen 1968; Hammarstrand 1980; Schaefer and Livingston 1990; Cavanaugh et al. 2015).

In developing our analysis methodology, we recognize not only that the frequency and the intensity of rain must clearly be distinguished, but, more importantly, that the rain frequency (probability), as well as other statistics, depends on the rain intensity. For this reason, we are going to systematically investigate the probabilistic variables as functions of the rain intensity. We introduce a threshold for defining accumulated rain events, and the rain statistics are investigated systematically by changing the rain thresholds over a full available range.

The present study supplements the already-existing different lines of investigations on the relation between the moisture and rain. Of particular importance is from a point of view of the criticality, as reviewed by Yano and Plant (2012, see especially sections 6.4 and 6.6), and Yano et al. (2014, see Q1.7). See e.g., Schiro et al. (2016), Kuo et al. (2017) for more recent developments. Another line of investigations emerges from a point of view of dynamical systems (Yano et al. 2020). Other recent significant contributions on rain–moisture relations include Ahmed and Schumacher (2015), Mapes et al. (2018), Powell (2019).

The focus on the rain–moisture relation in the present study is deliberate: the rain is certainly influenced by many other processes, as partially discussed in the final section, which are hardly measured only by moisture. Take convection, for example, as one of the processes contributing to rains: Yano et al. (2013), for example, discuss the processes contributing to the convection intensity in parameterization context.

The present paper proceeds as follows. After describing the analysis data in the next section, the methodologies, as well as theories behind, are introduced in section 3. The results are presented in section 4. It is followed by concluding discussions in section 5. Data uncertainties are discussed separately in the appendix. Further discussion and figures, though related but secondary in the present study, are provided as online supplemental information so that the main text can focus on the main theme of the study just introduced.

2. Data description

The area chosen for the study is Friuli Venezia Giulia (FVG), a region of northeast Italy, facing the Eastern Alps to the north, and the Grado and Marano Lagoons of the Adriatic Sea to the south (Fig. 1). Due to this unique topography, FVG is one of the areas experiencing the severest rains in central Europe (e.g., Feudale and Manzato 2014; Isotta et al.

2014; Manzato et al. 2016, 2019; Poelman et al. 2016; Pavan et al. 2019). The weather over FVG is characterized by two major regimes (cf. Siccardi 1996). From May to September (convective season), during which the Azores high over the Atlantic maintains a relatively stable synoptic state, most of rains are due to localized convection; these rains tend to be short, but can be very intense with up to 100 mm of accumulated rain over 1 h. From October to April (non-convective season), polar cold fronts frequently invade the region, often leading to persistent intense rains. Due to the support of synoptic systems, rainy days are more frequent, and 6-h-accumulated rains tend to be heaviest during autumn (cf. Fig. 5b of Manzato et al. 2016; see also Figs. 3 and 7 below).

The 12-yr-long dataset, spanning from 1 January 2006 to 1 January 2018, of soundings and rain gauges over the FVG Plain is adopted: a network of 33 mesonet (rain gauge) stations and a radiosounding station (WMO code 16044, managed by Italian *Aeronautica Militare*) near Udine.

The soundings are made every 12 h, at 0000 and 1200 UTC. For the analysis, the moistness of the atmosphere is measured by column precipitable water (CPW, in mm), i.e., vertical integral of the moisture density from these soundings, as defined in the next section by Eq. (1). A radiosonde typically traverses over a distance of the whole FVG Plain, stretching 80 and 40 km, respectively, in longitude and latitude, depending on the wind direction, taking on average 42 min before reaching the tropopause from the surface. As a result, the CPWs obtained from soundings are better considered to *statistically* represent FVG–Plain width values, rather than those of the local vertical column immediately above the sounding launch site.

Soundings were performed with Vaisala RS92, which has accuracy limits (maximum possible errors) of 0.3 K and 3%, respectively, for the temperature and the relative humidity (Vaisala 2013, see also Vömel et al. 2007; Miloshevich et al. 2009). The 0.3-K error in temperature contributes to 1% error to the saturated mixing ratio, thus the total of 4% maximum possible errors to CPW by adding the relative humidity errors. This amounts to the maximum possible errors of 50 mm × 0.04 = 2 mm for CPW.

The 6-hourly accumulated rains [mm (6 h)$^{-1}$], ending at 0000, 0600, 1200, and 1800 UTC, is available from the 33 FVG mesonet rain gauge stations, as listed in Table 1. The minimum detectable accumulated rain is 0.1 or 0.2 mm depending on the different gauge sensitivity: the rain is accumulated in pluviometer until it reaches the minimum detectable level. The minimum rain, 0.1–0.2 mm (6 h)$^{-1}$, is recorded in this manner, but with substantial errors due to the recording method as well as instrumentation issues.

In the following analysis, the rain observed at these rain gauge stations are individually paired with the CPW data, leading to 33 pairs of time series consisting of CPW and rain. Here, more precisely, the CPW values computed from the soundings at 0000 and 1200 UTC are paired with accumulated rains [mm (6 h)$^{-1}$] measured by 33 rain gauge stations over 0000–0600 and 1200–1800 UTC, respectively. This timing for pairing gives the highest correlation, especially more so than with rains over 1800–0000 and 0600–1200 UTC, respectively.

The resulting total is 265 813 pairs of measurements of sounding and rain gauge data. Here, 8756 soundings are available in total, whereas the numbers of available 6-hourly accumulated rain measurements from the stations for the same period are listed as the last column in parentheses in Table 1. The resulting total numbers of available sounding–rain data pairs are listed immediately to the left. The analyses are performed for the full period by default (full year), but also repeated by dividing the data into the convective (May–September) and non-convective (October–April) seasons.

The present study uses direct observational measurements, rather than commonly available analysis data, because the former is free of possible contaminations due to statistical interpolations as well as forecast-model dependencies in the data-assimilation procedures (Kalnay 2002). Furthermore, ECMWF forecast data tends to underestimate the most intense rains over the FVG Plain (Manzato et al. 2016, 2019).

3. Analysis methodology and probability theory

a. Column precipitable water

We measure the amount of moisture available in the atmosphere by the column precipitable water (CPW) I, which is defined by a vertical integral of the water vapor content in a given column atmosphere:

$$I = \frac{1}{\rho_w}\int_{z_s}^{z_T} \rho q_v \, dz = \frac{1}{\rho_w g}\int_{p_T}^{p_s} q_v \, dp. \tag{1}$$

Here q_v is the specific humidity, and ρ_w and ρ are the densities of liquid water and air, respectively. The vertical integral in height z is performed from the surface z_s to a top z_T (12 km in the present study), of a sounding measurement. The second expression is obtained from the first with a help of the hydrostatic balance ($dp/dz = -g\rho$), in which the integral is in terms of the pressure p with a reversed integral range. Here, g is the acceleration of the gravity.

In the following, by default, the analyses are performed over a range of CPW, $(I_1, I_2) = (5, 50)$ mm, and this range is divided into 18 discrete bins with a size of $\Delta I = 2.5$ mm. Each bin is characterized by its center value. As an alternative measure of moisture, section S.1 of the supplemental material considers separately the mean relative moisture (MRH as defined in Manzato 2005).

b. Probability theory: Definitions

In this study, the terms "probability" (or "chance") and "frequency" are used in interchangeable manner. Practically, the frequency, $p(I)$, say, of observing CPW I is evaluated by dividing a number, $N(I)$, of occurrences over a bin range $[I - \Delta I/2, I + \Delta I/2]$, by total number of data, N, i.e., $p(I)\Delta I = N(I)/N$. It is then reinterpreted as a probability.

The "rain state" (or "rain event") is defined as a state with rain R above a prefixed threshold R_c (>0), i.e., $R > R_c$. As already emphasized in the introduction, our goal is to investigate the change of the rain statistics with increasing rain threshold R_c. The behavior of intense rains is not necessarily

TABLE 1. List of 33 rain gauge stations adopted in the study. The number of data points listed is that of rain–CPW data pair available from each station with the total number of rain measurements available over 0000–0600 and 1200–1800 UTC separately given in parentheses. The former is further reduced due to missing soundings.

Station No.	Station name	Lon (°E)	Lat (°N)	No. of data points	
1	Brugnera	12.55	45.92	8660	(8715)
2	Forcate	12.59	45.99	8548	(8602)
3	Aviano	12.60	46.06	6231	(6270)
4	Porcia	12.61	45.92	5244	(5278)
5	Pordenone–MICROS	12.64	45.95	8657	(8712)
6	Pordenone–CAE	12.68	45.95	8682	(8738)
7	Cordenons	12.70	46.00	6365	(6404)
8	Vivaro	12.77	46.08	8688	(8744)
9	Basaldella di Vivaro	12.79	46.09	6315	(6354)
10	Mure	12.80	45.82	8680	(8735)
11	San Vito al Tagliamento–MICROS	12.82	45.90	8700	(8756)
12	Arba	12.82	46.12	8660	(8715)
13	San Vito al Tagliamento–CAE	12.87	45.92	8640	(8695)
14	Spilimbergo	12.88	46.10	6352	(6391)
15	Vacile	12.89	46.13	8604	(8658)
16	Codroipo	13.00	45.95	8689	(8745)
17	San Daniele del Friuli	13.01	46.15	8680	(8735)
18	Rivolto	13.02	45.95	8662	(8717)
19	San Mauro del Friuli	13.02	46.14	7260	(7299)
20	Pantianicco	13.04	46.01	7221	(7260)
21	Fagagna	13.07	46.10	8678	(8734)
22	Talmassons	13.16	45.88	8690	(8746)
23	Alnicco	13.16	46.12	8653	(8708)
24	Udine	13.23	46.04	8628	(8683)
25	Pavia di Udine	13.29	45.99	6714	(6753)
26	Povoletto	13.30	46.12	6246	(6285)
27	Palmanova	13.33	45.91	8655	(8710)
28	Cervignano	13.34	45.85	8667	(8723)
29	Cividale–CAE	13.42	46.09	8650	(8705)
30	Cividale–MICROS	13.42	46.08	8672	(8727)
31	Gradisca Dïis	13.48	45.89°	8684	(8740)
32	La Baita	13.50	45.94°	8674	(8728)
33	Capriva	13.51	45.96	8664	(8720)
	Total	—	—	265 813	(267 485)

identical to that of weak rains. We are going to elucidate this aspect. The change of the rain behavior with increasing intensities may be interpreted in analogy with the change of the characteristics of the hydrodynamics instabilities with increasing perturbation amplitudes (Drazin and Reid 1981): when the perturbation amplitude is weak enough, it can be analyzed by assuming an infinitesimal amplitude. However, as the perturbation amplitude increases, finite-amplitude effects become significant: the system gradually transits form a linear to nonlinear regime. An analogous perspective can be adopted for transition of regimes with the rain statistics, and also analogous terminologies of infinitesimal and finite regimes, although the distinction may not be taken in the literal sense, as the rainfall process is arguably inherently nonlinear.

To investigate dependence of rain on moisture, the most basic to consider is the average rain, $\overline{R}(I)$, under a given CPW, I:

$$\overline{R}(I) = \int_0^{+\infty} p(R|I) R \, dR. \tag{2}$$

Here $p(R|I)$ is the conditional probability density of rain R with a given CPW I, which is further related to the joint probability density of I and R [denoted $p(I, R)$] and the probability density of I [denoted $p(I)$] by

$$p(R|I) = p(I, R)/p(I). \tag{3}$$

The present study further divides the dependence of rain on moisture into two contributions: the first is the change of the probability of rain (with $R > R_c$) with increasing CPWs, I:

$$P(R > R_c|I) = \int_{R_c}^{+\infty} p(R|I) dR. \tag{4}$$

Here note that the probability density and the probability are distinguished by the lowercase and the uppercase letters, respectively, p and P.

The second is a change of the expected rain intensity $\overline{R}(R > R_c, I)$ with increasing CPWs, I:

$$\overline{R}(R > R_c, I) = \int_{R_c}^{+\infty} p(R|R > R_c, I) R\, dR, \tag{5}$$

with the rain state defined by the condition $R > R_c$. In words, $\overline{R}(R > R_c, I)$ is the intensity of the rain expected under the conditions of $R > R_c$ with a given CPW.

In the following data analysis, $\overline{R}(I)$ is evaluated by averaging all the rain measurements available over the bin range, $[I - \Delta I/2, I + \Delta I/2]$; $P(R > R_c|I)$ by counting the number of occurrences, $N(R > R_c, I)$, with $R > R_c$ over $[I - \Delta I/2, I + \Delta I/2]$, i.e., $P(R > R_c|I) = N(R > R_c, I)/N(I)$; $\overline{R}(R > R_c, I)$ by averaging over all the available rain measurements with $R > R_c$ over $[I - \Delta I/2, I + \Delta I/2]$.

c. Rain-state statistics

Since our interest is the change of rain behavior with increasing CPWs, it is sometimes helpful to focus only on the statistics for the rain state, defined by $R > 0$ [or more precisely, $R \geq 0.1$ or 0.2 mm $(6\text{ h})^{-1}$ with the present data]. For example we may consider the rain-state joint probability, $p(I, R|R > 0)$, instead of the full joint probability $p(I, R)$. Note that the former is related to the latter by the relation:

$$p(I, R|R > 0) = p(I, R)/P(R > 0). \tag{6a}$$

Similarly, we also find

$$p(R|I, R > 0) = p(R|I)/P(R > 0|I). \tag{6b}$$

Thus, constraining our attention to the rain state merely has a consequence of multiplying a distribution by a constant probability factor, but otherwise the distribution form itself is not affected.

Moreover, realize that $p(I, R = 0)$ and $p(R = 0|I)$ as probability densities are rather ill defined for the two reasons:

1) If it is ever possible to define an absolute zero-rain state strictly, at least conceptually, we should have a finite chance for this state, thus the probability $P(R = 0|I)$, rather than its density counterpart, would have a finite value. It follows that

$$p(R = 0|I) = \lim_{\Delta R \to 0} \frac{P(R \leq \Delta R|I)}{\Delta R} = P(R = 0|I) \lim_{\Delta R \to 0} \frac{1}{\Delta R} \to \infty,$$

because $\lim_{\Delta R \to 0} P(R \leq \Delta R|I) = P(R = 0|I) \neq 0$. Thus, $p(R = 0|I)$ is singular, so is $p(I, R = 0)$.

2) Practically speaking, it is very difficult to establish an asymptotic tendency of the probability densities $p(I, R)$ and $p(R|I)$ toward $R \to 0$, because it is difficult to measure extremely weak rains accurately. For example, with the rain gauge used in the present study, the drizzle events with less than 0.1 mm $(6\text{ h})^{-1}$ are not recorded.

Technically, it would be possible to put the zero–rain statistics into the first bin of the counting, i.e., $0 \leq R \leq 0.1$ mm $(6\text{ h})^{-1}$, for evaluating $p(I, R)$ and $p(R|I)$. However, in that case, the first bin value becomes singularly larger than the other bins. For this reason, we instead consider $p(I, R|R > 0)$ and $p(R|I, R > 0)$ in the following. Note that the equivalent relations to Eqs. (6a) and (6b) are applicable also when a nonzero rain threshold, $R_c(\neq 0)$ is assumed. Thus, the discussion of this subsection also demonstrates the self-consistency of the analysis with a nonzero threshold (i.e., $R_c \neq 0$) in the following.

d. Probability theory: Relations

We can interpret that the average rain $\overline{R}(I)$ under a given CPW I is determined from the two major contributions: the rain probability $P(R > R_c|I)$ and the expected rain intensity $\overline{R}(R > R_c, I)$ as seen in the following manner. First note that the joint probability density, of R and $R > R_c$ under a given I $[p(R, R > R_c|I)]$ can be written two different ways:

$$p(R, R > R_c|I) = p(R|R > R_c, I)P(R > R_c|I) = P(R > R_c|R, I)p(R|I).$$

Here, $P(R > R_c|R, I) = 1$ when $R > R_c$, and otherwise both $p(R, R > R_c|I)$ and $P(R > R_c|R, I)$ are simply zero, making the relation trivial. Thus, it immediately follows that

$$p(R|R > R_c, I) = \frac{p(R|I)}{P(R > R_c|I)}.$$

Moreover, $P(R > R_c|I)$ does not depend on R. Thus, Eq. (5) reduces to

$$\overline{R}(R > R_c, I) = \frac{\int_{R_c}^{+\infty} p(R|I) R\, dR}{P(R > R_c|I)}. \tag{7}$$

Note especially when $R_c = 0$, the above expression simply reduces to

$$\overline{R}(R > 0, I) = \frac{\overline{R}(I)}{P(R > 0|I)}, \tag{8}$$

i.e., the average rain, under rain conditions ($R > 0$) and with a given CPW I is obtained by dividing the average rain with the probability of rain ($R > 0$) both under a given CPW.

To see a more general relation than Eq. (8) between the three basic quantities (2), (4), and (5), we rewrite Eq. (2) as

$$\overline{R}(I) = \int_0^{R_c} p(R|I) R\, dR + \int_{R_c}^{+\infty} p(R|I) R\, dR.$$

Noting that

$$P(R < R_c|I) = 1 - P(R > R_c|I),$$

and recalling the definition of the conditional average, (7), this expression further reduces to

$$\overline{R}(I) = P(R > R_c|I)\overline{R}(R > R_c, I) + \left[1 - P(R > R_c|I)\right]\overline{R}(R \leq R_c, I). \tag{9}$$

This is a general formula showing how the rain probability $P(R > R_c|I)$ and the expected rain intensity $\overline{R}(R > R_c, I)$ contribute in defining the average rain $\overline{R}(I)$.

Although the general expression (9) is more involved, we may note that the second term becomes smaller as taking the limit toward $R_c \to 0$ asymptotically, because $\overline{R}(R \le R_c, I) \to 0$. Thus, we expect that

$$\overline{R}(I) \simeq P(R > R_c|I)\overline{R}(R > R_c, I) \tag{10}$$

is still a good approximation, when the threshold R_c is small enough, and we essentially recover Eq. (8).

Furthermore, an exact version of Eq. (10) can be derived by introducing the average above-threshold rain defined by

$$\overline{R}_+(I|R_c) \equiv \int_{R_c}^{+\infty} p(R|I)R\,dR. \tag{11}$$

Then, we find

$$\overline{R}_+(I|R_c) = P(R > R_c|I)\overline{R}(R > R_c, I). \tag{12}$$

This is an exact general relationship between the average (left-hand side) and the expected intensity (on the right-hand side).

Note that $\overline{R}_+(I, R_c)$ is the average of the above-threshold rain $R_+(R_c)$, which is obtained by retaining only the states with $R > R_c$, and otherwise setting as zero rain:

$$R_+(R_c) = \begin{cases} R, & R > R_c, \\ 0, & R \le R_c. \end{cases} \tag{13}$$

The analysis in the next section focusing of the rain statistics with finite thresholds $R_c > 0$ can be interpreted as an analysis of the above-threshold rain $R_+(R_c)$ defined by Eq. (13).

An example of the above-threshold rain time series [at Udine for the last 100 days of the first year of data with R_c = 10 mm (6 h)$^{-1}$] is shown in Fig. 2b to be compared with the full rain time series in Fig. 2a. Construction of the above-threshold rain [Eq. (13)] may appear artificial by deliberately excluding weaker rains from the time series. However, the procedure can simply be interpreted as a type of filtering (Lilly 1967; Leonard 1975; Reynolds 1990, chapter 13 of Pop 2000, section 3.3 of Yano 2015).

e. Statement of the problem

Our key question is how the conditional probability $P(R > R_c|I)$ and the expected rain intensity $\overline{R}(R > R_c, I)$ contribute in defining the average rain, $\overline{R}(I)$, under a given CPW, I. Based on Eq. (12), this question is better posed in terms of the average above-threshold rain $\overline{R}_+(I|R_c)$ rather than $\overline{R}(I)$.

f. Sensitivity analysis

Differentiating both sides of Eq. (12) by CPW I, we obtain after some rearrangements:

$$\frac{\Delta I}{\overline{R}_+(I|R_c)}\frac{\partial \overline{R}_+(I|R_c)}{\partial I} = \frac{\Delta I}{P(R > R_c|I)}\frac{\partial P(R > R_c|I)}{\partial I} + \frac{\Delta I}{\overline{R}(R > R_c, I)}\frac{\partial \overline{R}(R > R_c, I)}{\partial I}, \tag{14}$$

with $\Delta I = I_2 - I_1$(=45 mm) being the analysis range. Thus, the normalized tendency of $\overline{R}_+(I|R_c)$ (left-hand side) is defined by a sum of the normalized tendencies of $P(R > R_c|I)$ and $\overline{R}(R > R_c, I)$, as given on the right-hand side as the first and the second terms. Thus, we can conclude that the normalized local tendencies defined by

$$\frac{\Delta I}{P(R > R_c|I)}\frac{\partial P(R > R_c|I)}{\partial I} \tag{15a}$$

and

$$\frac{\Delta I}{\overline{R}(R > R_c|I)}\frac{\partial \overline{R}(R > R_c|I)}{\partial I} \tag{15b}$$

provide measures for the contributions of the rain probability $P(R > R_c|I)$ and the expected intensity $\overline{R}(R > R_c|I)$ to the average above-threshold rain $\overline{R}_+(I|R_c)$ and, to a lesser extent, to the average rain $\overline{R}(I)$ for a given CPW I recalling the asymptotic relation (10).

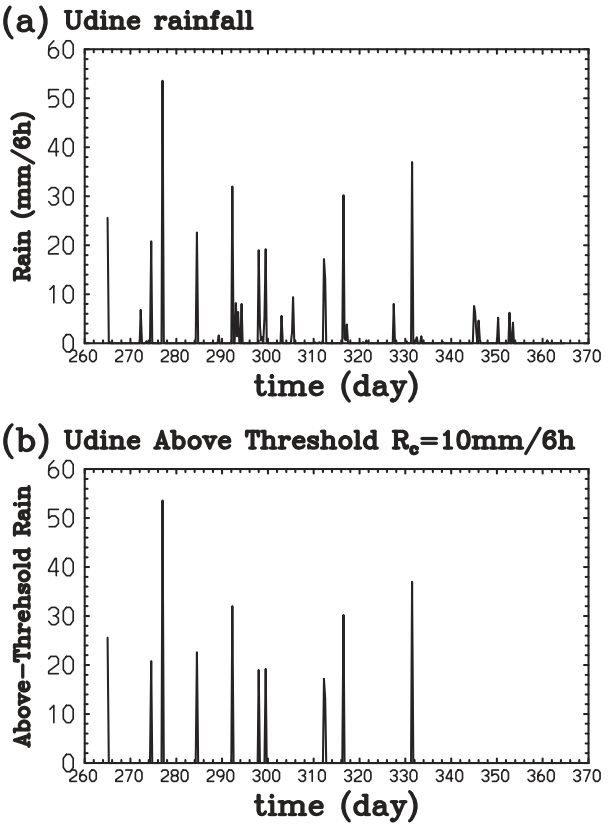

FIG. 2. The Udine rain during the last 100 days of the first year (2006): (a) as measured by the rain gauge [mm (6 h)$^{-1}$] and (b) the "above-threshold" rain [above the threshold R_c = 10 mm (6 h)$^{-1}$].

4. Results

As stated in section 3e, our key question is the change of the dependencies of $P(R > R_c|I)$ and $\overline{R}(R > R_c, I)$ on I with the increasing R_c. However, to set the scene properly, we first examine the more basic variables $\overline{R}(I)$ and $\overline{R}_+(I|R_c)$.

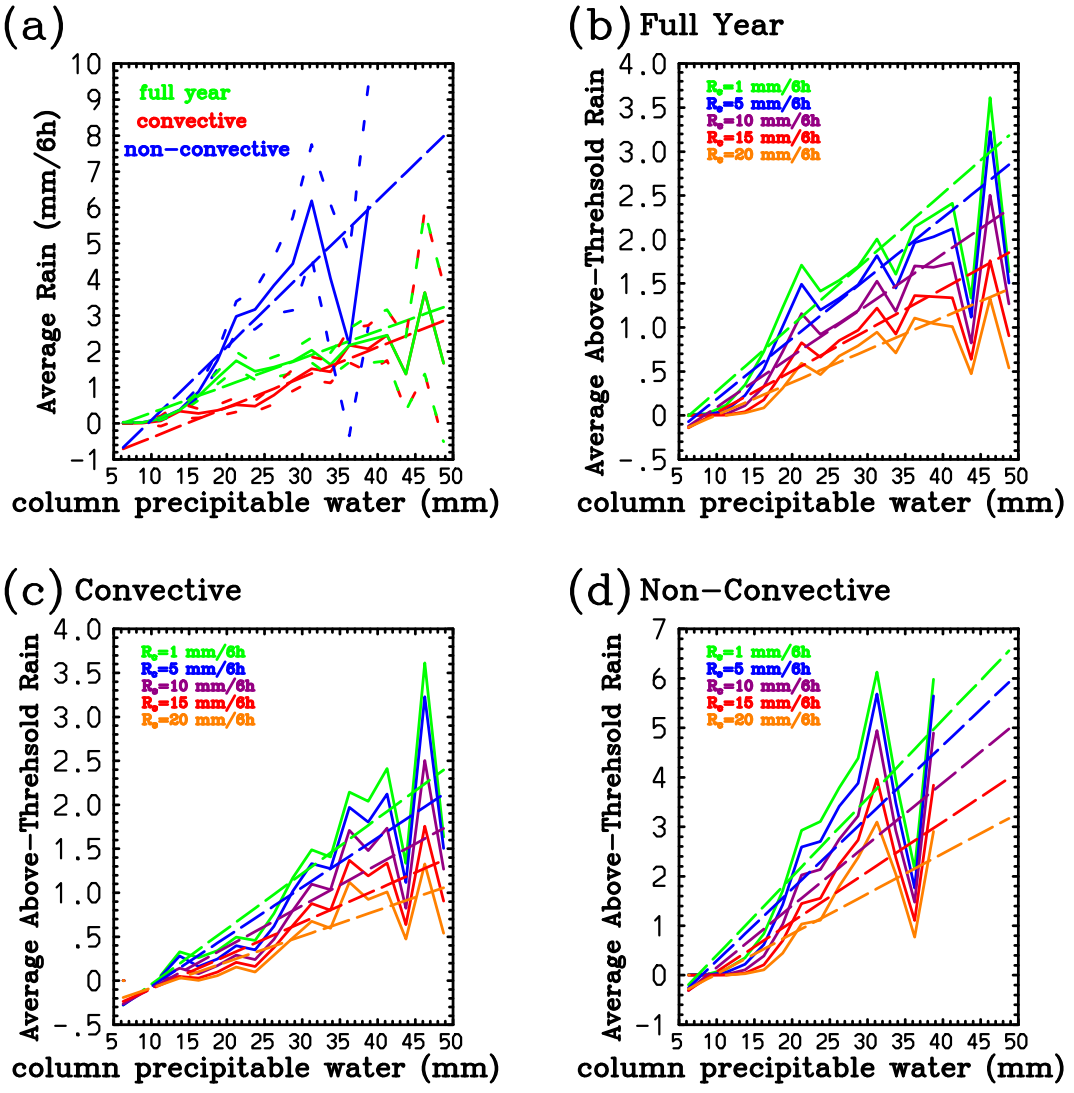

FIG. 3. (a) Average rain $\overline{R}(I)$ [mm (6 h)$^{-1}$] with a given CPW I for the full year (green), convective (red), and non-convective seasons (blue), with all 33 rain gauge stations. (b)–(d) Average above-threshold rain $\overline{R}_+(I|R_c)$ defined with the thresholds $R_c = 1$ (green), 5 (blue), 10 (violet), 15 (red), and 20 mm (6 h)$^{-1}$ (orange) for (b) full year, (c) convective seasons, and (d) non-convective seasons. Least square linear fits are shown by long-dashed lines. In (a), the upper and lower bounds of data uncertainties, based on a method described in the appendix, are further marked by short-dashed curves.

a. Rain dependence on CPW

Figure 3a shows the average rain $\overline{R}(I)$ with a given CPW I for the 33 rain gauge stations for the full years (green), as well as for convective (red) and non-convective (blue) seasons. They increase overall with increasing CPWs, and also overall linearly, as suggested by long-dashed lines of least square fits. In performing the least square fits to straight lines, here and hereinafter, the statistical points are weighted by the numbers of measurements used for the evaluation. This weighting properly takes into account the uncertainty associated with small numbers of data over the tails of the CPW distribution. Furthermore, the upper and lower bounds of data uncertainties, as estimated in the appendix, are marked by short-dashed curves.

The result seems to support a popular belief that more moisture leads to more rains (cf. Khodayar et al. 2018; Grazzini et al. 2020). This conclusion does not change regardless of whether we focus on particular seasons. We may also note a twice steeper slope for the non-convective winter season with frequent arrivals of cold fronts: twice more rain is expected with $I > 15$ mm on average during winter than summer.

Figure 3 further shows the average above-threshold rain $\overline{R}_+(I|R_c)$ defined by Eq. (11) for the full year (Fig. 3b), convective seasons (Fig. 3c), and non-convective seasons (Fig. 3d) with varying rain thresholds R_c = 1–20 mm (6 h)$^{-1}$. Linear fits are also shown by long-dashed lines. We find that the curves for $\overline{R}_+(I|R_c)$ remain similar to that of $\overline{R}(I)$, but with reductions of slopes with increasing thresholds, R_c. In

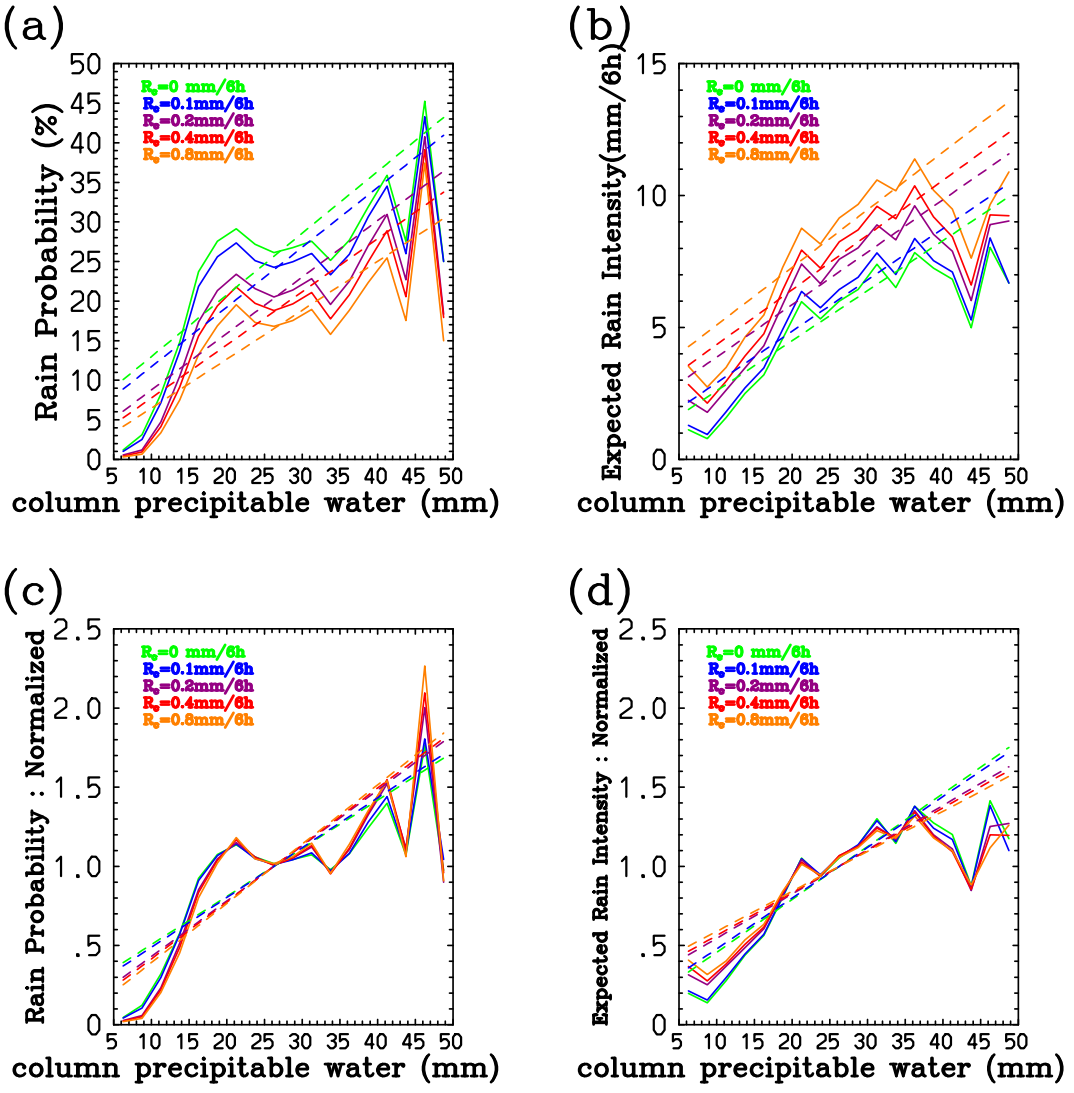

FIG. 4. Statistics of rain gauge data for the full period with smaller thresholds [$R_c < 1$ mm (6 h)$^{-1}$]. (a) Probability (frequency) of rain $P(R > R_c|I)$ under a given rain threshold R_c. (b) The expected rain intensity $\overline{R}(R > R_c, I)$ with the rain condition defined by $R > R_c$. (c),(d) As in (a) and (b), respectively, but with normalization. The curves are for the rain thresholds $R_c = 1$ (green), 5 (blue), 10 (violet), 15 (red), and 20 mm (6 h)$^{-1}$ (orange). Linear least square fits are also shown by short-dashed lines.

other words, the characteristics of the average rain with increasing CPWs are well preserved, even when the rain less than R_c is truncated to zero as in Eq. (13).

Issues concerning the degree of spatial variability of rains over FVG depending on CPW are addressed in section S.2 of the supplemental material.

b. Rain probability and the expected intensity

The average rains $\overline{R}(I)$ and $\overline{R}_+(I|R_c)$ under a given CPW are controlled by two major factors: the probability for rain $P(R > R_c|I)$ and the expected intensity of rain for the events $\overline{R}(R > R_c, I)$ as suggested by an asymptotic formula, (10), as well as the relation (12). We, thus, examine how these two factors contribute to increasing rains with increasing CPWs.

The threshold dependencies are investigated for the range of R_c = 0–20 mm (6 h)$^{-1}$ in the following, but with separate figures for the infinitesimal [$R_c < 1$ mm (6 h)$^{-1}$] and finite [$R_c \geq 1$ mm (6 h)$^{-1}$] regimes, for a better clarity of the presentation. Figures 4a and 5a show that the conditional frequency, *or* probability $P(R > R_c|I)$, of rain indeed increases with increasing available moistures in the atmosphere, *or* CPWs, with varying thresholds, R_c. Here, the 33 rain gauge stations are considered for the full year. The probability $P(R > R_c|I)$ overall increases linearly with increasing CPWs, as suggested by short-dashed lines for least square fits, with values for fitting listed in Table 2. Furthermore, the rain probability

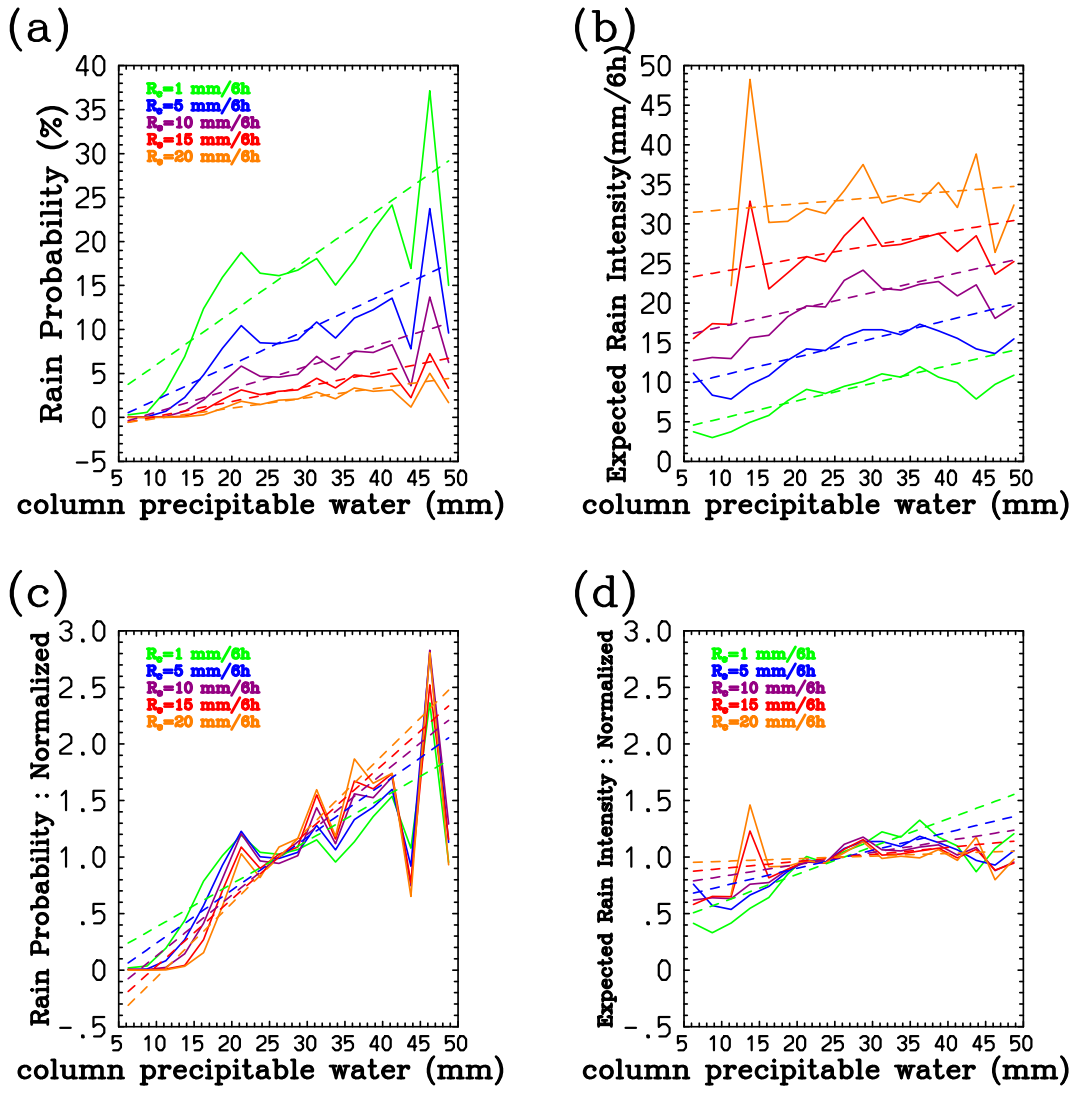

FIG. 5. As in Fig. 4, but with larger thresholds [$R_c \geq 1$ mm $(6\ \mathrm{h})^{-1}$].

decreases with increasing rain thresholds R_c at a rate almost independent of CPW.

Figures 4b and 5b, in turn, plot the expected rain intensity $\overline{R}(R > R_c, I)$ as a function of CPW with varying rain thresholds R_c superposed by short-dashed lines for linear least square fits. Particularly noticeable is positive finite expected-rain intensities as $I \to 0$ obtained by extrapolating the linear fits, which increase with increasing thresholds R_c as listed in Table 2, although the rain probability itself vanished at $I = 0$.

There is an increasing tendency of $\overline{R}(R > R_c, I)$ with increasing CPWs I over the full range of R_c. However, the more quantitative behavior changes with the increasing R_c: over the infinitesimal regime [$R_c < 1$ mm $(6\ \mathrm{h})^{-1}$], the expected rain intensity $\overline{R}(R > R_c, I)$ overall increases at the same rate independent of the threshold R_c (Fig. 4b). These increasing tendencies are compared well with those with the probability $P(R > R_c|I)$ found in Fig. 4a.

There is a clear transition of the regime by further increasing the threshold R_c: with a finite rain with $R_c \geq 1$ mm $(6\ \mathrm{h})^{-1}$, the increasing tendency of $\overline{R}(R > R_c, I)$ with the increasing CPW I becomes less noticeable, and even in a lesser degree with increasing thresholds R_c: these weak dependencies on CPW are overall smaller than data uncertainties, as suggested in the appendix (cf. Fig. A2b). In other words, an increasing tendency of the expected intensity $\overline{R}(R > R_c, I)$ over the finite regime with increasing CPWs is less significant than that for the average rain $\overline{R}(I)$ (cf. Fig. 3), especially when more intense rains are considered: although more moisture may somehow favor more intense rains, this tendency is *less pronounced* than for the rain probability.

To see the overall tendencies of $P(R > R_c|I)$ and $\overline{R}(R > R_c, I)$ more clearly, the curves in Figs. 4a, 4b, 5a, and 5b are replotted in Figs. 4c, 4d, 5c, and 5d by normalizing them by $P(R > R_c|I_0)$ and $\overline{R}(R > R_c|I_0)$ of the linear fits with

TABLE 2. The least square linear fits of $P(R < R_c|I)$ and $\overline{R}(R < R_c, I)$. Values at $I = 0$ and the slopes for both variables for a given threshold R_c at each row.

R_c [mm (6 h)$^{-1}$]	$\overline{R}(R < R_c, I = 0)$ (%)	$dP(R < R_c\|I)/dI$ (% mm^{-1})	$\overline{R}(R < R_c, I = 0)$ [mm (6 h)$^{-1}$]	$d\overline{R}(R < R_c, I)/dI$ [(6 h)$^{-1}$]
0	5.2	0.78	0.70	0.19
0.1	4.2	0.75	0.96	0.19
0.2	1.6	0.71	1.9	0.20
0.4	1.0	0.67	2.2	0.20
0.8	0.29	0.62	2.9	0.22
1	1.2×10^{-2}	0.60	3.2	0.22
5	−2.0	0.40	8.5	0.23
10	−2.0	0.26	15	0.22
15	−1.6	0.17	22	0.17
20	−1.3	0.12	31	7.7×10^{-2}

$I_0 = (I_1 + I_2)/2 = 27.5$ mm. Also shown by the short-dashed lines are linear least square fits.

In the infinitesimal regime [$R_c < 1$ mm (6 h)$^{-1}$], comparable rates of increase of both $P(R > R_c|I)$ and $\overline{R}(R > R_c, I)$ with increasing I are much clearly seen after the normalization (Figs. 4c,d): all these curves superpose each other quite well after normalizations; we can safely conclude that all these normalized curves are identical within data uncertainties (discussed in the appendix). The slopes of the linear fits are also almost identical for both variables, although the actual curves may look slightly gentler with $\overline{R}(R > R_c, I)$.

In the finite regime [$R_c \geq 1$ mm (6 h)$^{-1}$], all these curves still superpose each other relatively well after normalizations (Figs. 5c,d), but to a lesser extent than in the infinitesimal regime. Although the actual curves fluctuate substantially, the overall tendencies of all these curves are relatively linear. The larger fluctuations for larger CPWs and larger thresholds, R_c, are likely due to data uncertainties with lack of sufficient data, as suggested in the appendix.

Furthermore, these normalized linear slopes in Figs. 5c and 5d are substantially gentler for the expected rain intensity $\overline{R}(R > R_c, I)$ than for the rain probability $P(R > R_c|I)$. It reiterates the point already suggested by Figs. 5a and 5b in a more objective manner: the increase of $P(R > R_c|I)$ with increasing CPWs is more pronounced than that of $\overline{R}(R > R_c, I)$. We further note that these slopes increase and decrease, respectively, for $P(R > R_c|I)$ and $\overline{R}(R > R_c, I)$ with increasing thresholds R_c. Thus, as we focus our attentions to more intense rains, as seen with the above-threshold rain $R_+(R_c)$ more moisture contributes more significantly to an increase of chance rather than to increasing rain magnitudes.

As discussed in section 3f, the dependencies of $\overline{R}_+(I|R_c)$ on $P(R > R_c|I)$ and $\overline{R}(R > R_c, I)$ can more directly be compared by plotting the normalized local tendencies [Eqs. (15a) and (15b)] as functions of CPW, I (Figs. 6 and 7). The normalized local tendencies can deviate substantially from the linear-fit slopes, and its degree tends to be more pronounced for $P(R > R_c|I)$ (solid curves) rather than for $\overline{R}(R > R_c, I)$ (short-dashed curves).

However, here also the contrast between the infinitesimal and finite regimes stands out: in the infinitesimal regime [$R_c <$ 1 mm (6 h)$^{-1}$], these two curves still overlap each other rather well (Fig. 6). Over a narrow range of I = 5–15 mm, the local slopes for $\overline{R}(R > R_c, I)$ are clearly smaller than those for $P(R > R_c|I)$, but only by half for the full year and the nonconvective seasons (Figs. 6a,c). During the convective seasons (Fig. 6b), these two curves fairly overlap over this range. All these are in support of the previous conclusion that both $P(R > R_c|I)$ and $\overline{R}(R > R_c, I)$ increase with the increasing CPW I with a similar rate: in the infinitesimal regime, both contribute equally to the increase of the $R_+(I|R_c)$, with the increasing moisture I.

On the other hand, in the finite regime (Fig. 7), the local slopes of $P(R > R_c|I)$ (solid curves) are much more pronounced than for $\overline{R}(R > R_c, I)$ (short-dashed curves) over the range of I = 5–20 mm, except for the convective season, in which values for $\overline{R}(R > R_c, I)$ over this range is simply missing (Fig. 7b). Thus, the increase of the average above-threshold rain $\overline{R}_+(I|R_c)$ with the increasing moisture is mostly due to that of the rain probability $P(R > R_c|I)$ rather than $\overline{R}(R > R_c, I)$. Large local tendencies of $P(R > R_c|I)$ over the range of I = 5–20 mm may loosely be interpreted as a rapid pickup, analogous to "transition to strong convection" found over the tropics (Neelin et al. 2009).

c. Probabilistic interpretation

As shown in section 3b, the conditional frequency distribution $p(R|I)$ of rain R for a given CPW I constitutes a basis for deriving the quantities considered in previous last two subsections: $\overline{R}(I)$ by Eq. (2), $P(R > R_c|I)$ by Eq. (4), and $\overline{R}(R > R_c, I)$ by Eq. (5). The conditional frequency distribution $p(R|I)$ is, in turn, defined by Eq. (3) from the joint frequency distribution $p(I, R)$ of the CPW I and the rain R.

To better interpret the relations between the rain and moisture identified so far, thus we next examine the joint frequency distribution $p(I, R|R > 0)$ of nonzero rains: it is plotted in Fig. 8a in terms of a number of occurrences per bin, i.e., $N_+p(I, R|R > 0)\Delta I\Delta R$, where N_+ is the total number of data with nonzero rain, ΔI = 2 mm and ΔR = 2 mm (6 h)$^{-1}$ are bin sizes for I and R, respectively. Here, data with zero rain are excluded to focus on the rain state, as discussed in section 3c. The rain occurs more frequently over the range of CPW, I = 10–35 mm. Heavy rain events, say, above 20 mm (6 h)$^{-1}$ are also most frequent over this range.

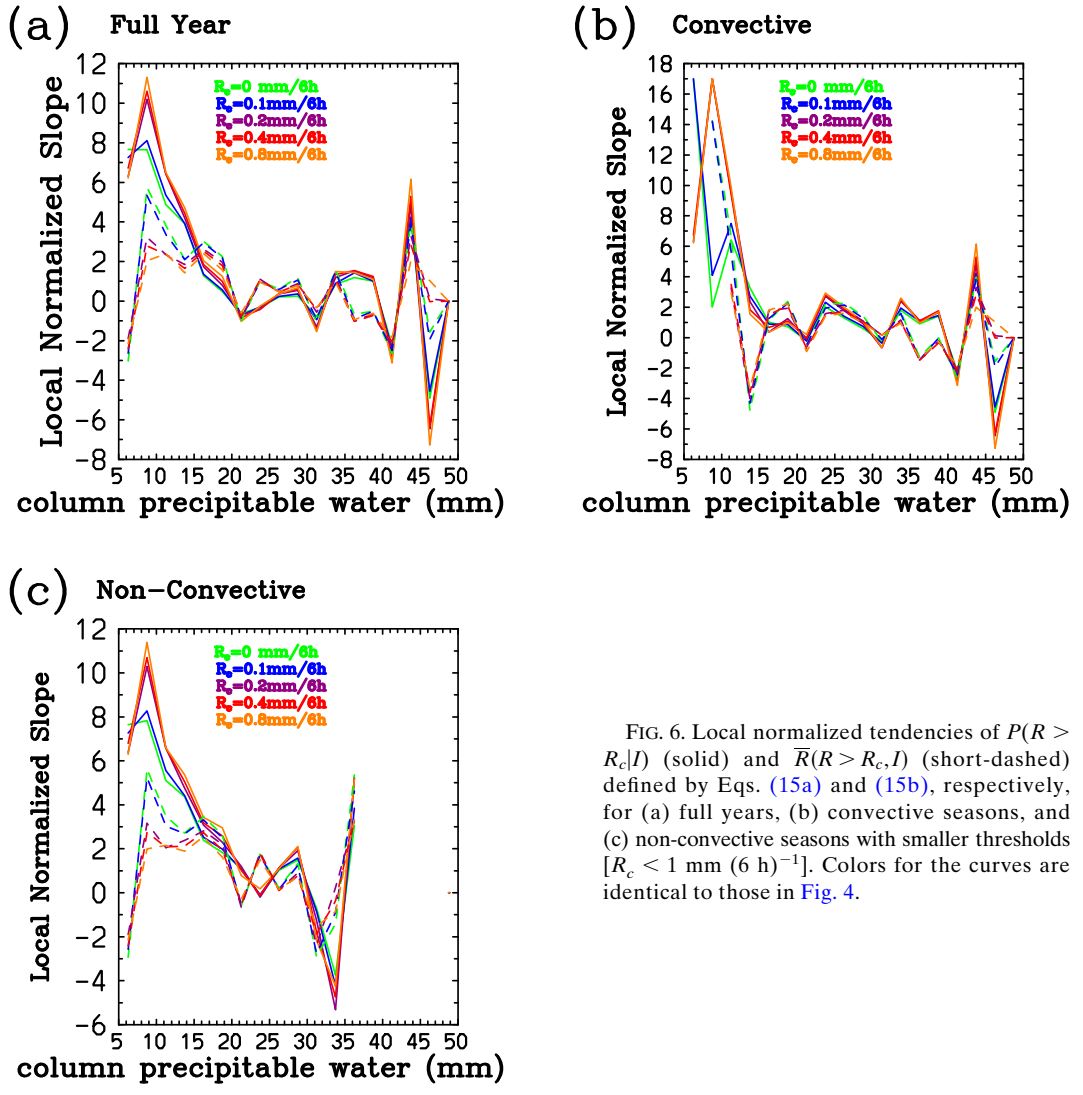

FIG. 6. Local normalized tendencies of $P(R > R_c|I)$ (solid) and $\overline{R}(R > R_c, I)$ (short-dashed) defined by Eqs. (15a) and (15b), respectively, for (a) full years, (b) convective seasons, and (c) non-convective seasons with smaller thresholds [$R_c < 1$ mm (6 h)$^{-1}$]. Colors for the curves are identical to those in Fig. 4.

However, it does not necessarily mean that the range of I = 10–35 mm, is the most optimal for producing the intense rains, because a frequent occurrence of rain is simply due to a more frequent occurrence of CPW values in this range: Fig. 8b shows a number of occurrences of CPW for every 2 mm bin, both including [$N(I)$, blue] and excluding [$N_+(I)$, red] the zero rain measurements.

Figure 8c, in turn, shows the conditional frequency distribution $p(R|I, R > 0)$ using the same bin size for the CPW as in Fig. 8a. Note that $p(I|R > 0)$ is directly obtained by dividing the red curve [$N_+(I)$] in Fig. 8b by the blue curve [$N(I)$]. After the transformation by Eq. (3), the distribution $p(R|I, R > 0)$ as shown in the vertical direction, no longer changes in any dramatic manner with a change of CPW, as moving in the horizontal direction. Most notably, we no longer see higher frequencies over the range of I = 10–35 mm, than other CPW ranges.

This distribution (Fig. 8c) more directly answers the question of whether a chance of intense rain actually increases with increasing CPWs. Here, we *do* see a slight tendency for more frequent intense rains with increasing CPWs. Nevertheless, any change of $p(R|I, R > 0)$ (Fig. 8c) with a change of CPW I with the fixed rain R is evidently less pronounced than that of $p(I, R|R > 0)$ (Fig. 8a). In other words, the *conditional* distribution $p(R|I, R > 0)$ is overall independent of CPW I in a relative sense, compared to a more significant dependency found in the *joint* distribution $p(I, R|R > 0)$.

To substantiate our claim, i.e., more moisture does not induce more intense rain in any substantial manner, the same is examined by plotting the frequency $p(R|I, R > 0)$ as histograms in Fig. 8d: the frequencies over a CPW bin of 10 mm are shown for a full range of CPW, I = 0–50 mm. They overlay each other rather well for the range of I = 20–50 mm. It simply suggests that, the statistical characteristics of rains are almost identical independent of the available moisture in the atmosphere when it is already moist enough (i.e., $I \geq 20$ mm). On the other hand, the rain frequency $p(R|I, R > 0)$ decreases with the increasing rain more rapidly for the smaller CPWs below I = 20 mm: to have a good chance of

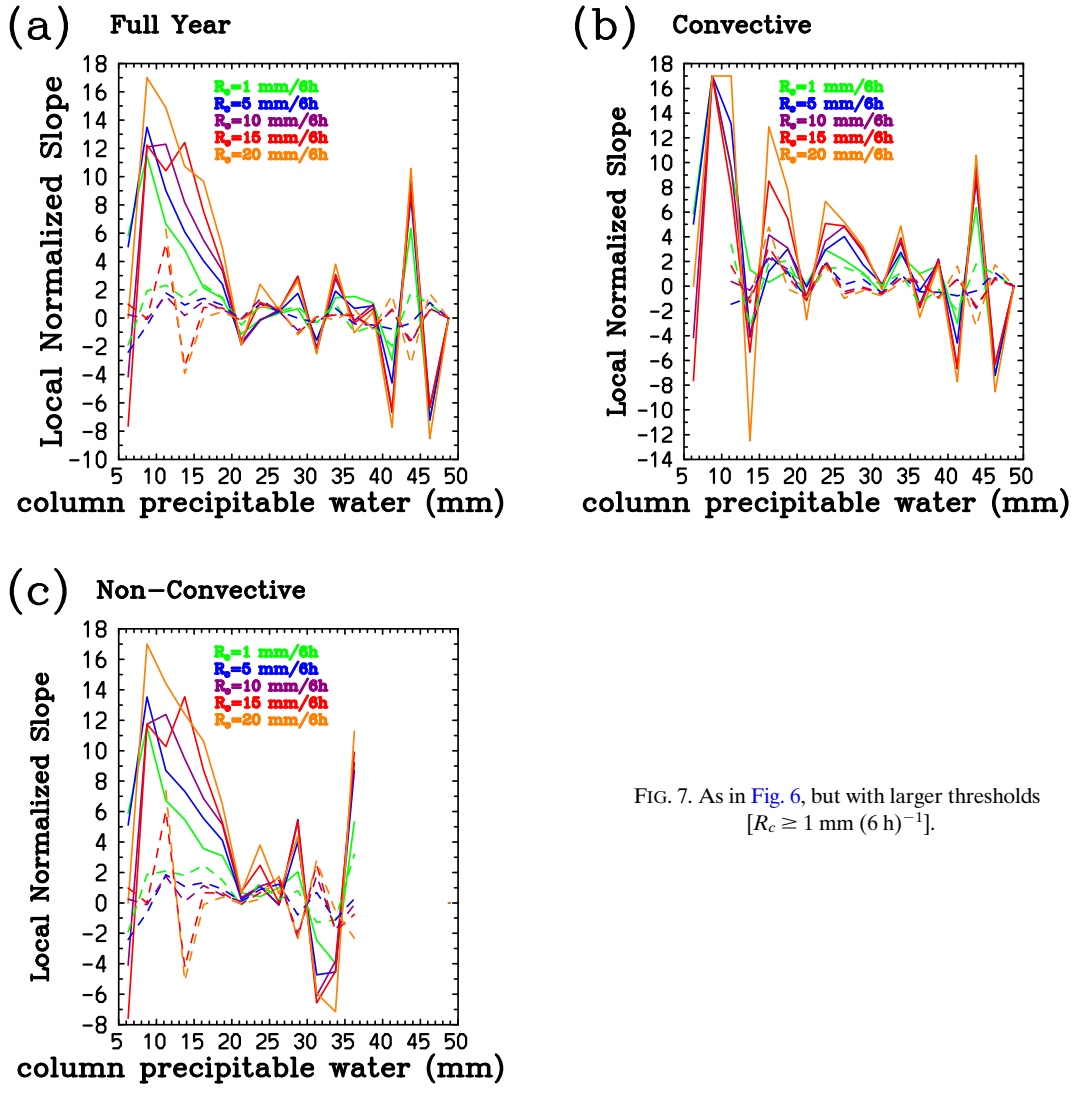

FIG. 7. As in Fig. 6, but with larger thresholds $[R_c \geq 1 \text{ mm } (6 \text{ h})^{-1}]$.

heavy rain, say, above 40 mm $(6 \text{ h})^{-1}$, CPW of at least 20 mm is required.

If the conditional probability $p(R|I, R > 0)$ is indeed independent of CPW for $I \geq 20$ mm as suggested by Fig. 8d, it has direct implications to the results of Fig. 5. First note that $P(R > R_c|I, R > 0)$ also becomes independent of I, because it is simply obtained by an integral of $p(R|I, R > 0)$. It follows from Eq. (7) that $\overline{R}(R > R_c, I)$ is also independent of I, for $I \geq 20$ mm apart from a constant depending only on R_c. (This conclusion is not inconsistent with the results of Figs. 5b and 5d within the data uncertainties suggested in Fig. A2d.) Conversely, for a "weak" dependence of the expected rain intensity on the CPW seen in Figs. 5b and 5d for $I \geq 20$ mm to be significant, a "weak" dependence of $p(R|I, R > 0)$ on I found in Fig. 8d must also be significant. Furthermore, independence of $P(R > R_c|I, R > 0)$ on I leads to identical distributions of $P(R > R_c|I)$ after normalizations as suggested by Fig. 5c. On the other hand, $P(R > R_c|I)$ still depends on I, because it is also proportional to $P(R > 0|I)$ as suggested by Eq. (6b).

5. Further discussion

The present study has examined a basis of a common notion that the amount of available moisture defines the rain. Here, the available moisture in the atmosphere is measured by the column precipitable water (CPW) in this study. An important element to investigate this question is the fact that the answer depends on the intensity of rains to consider. In this study, the rain events are defined as those above a threshold R_c, and all the probabilistic variables are evaluated being conditioned by this threshold.

A probabilistic formulation for addressing this question has been introduced (section 3), in which the key variables to examine are the conditional rain probability $P(R > R_c|I)$ and

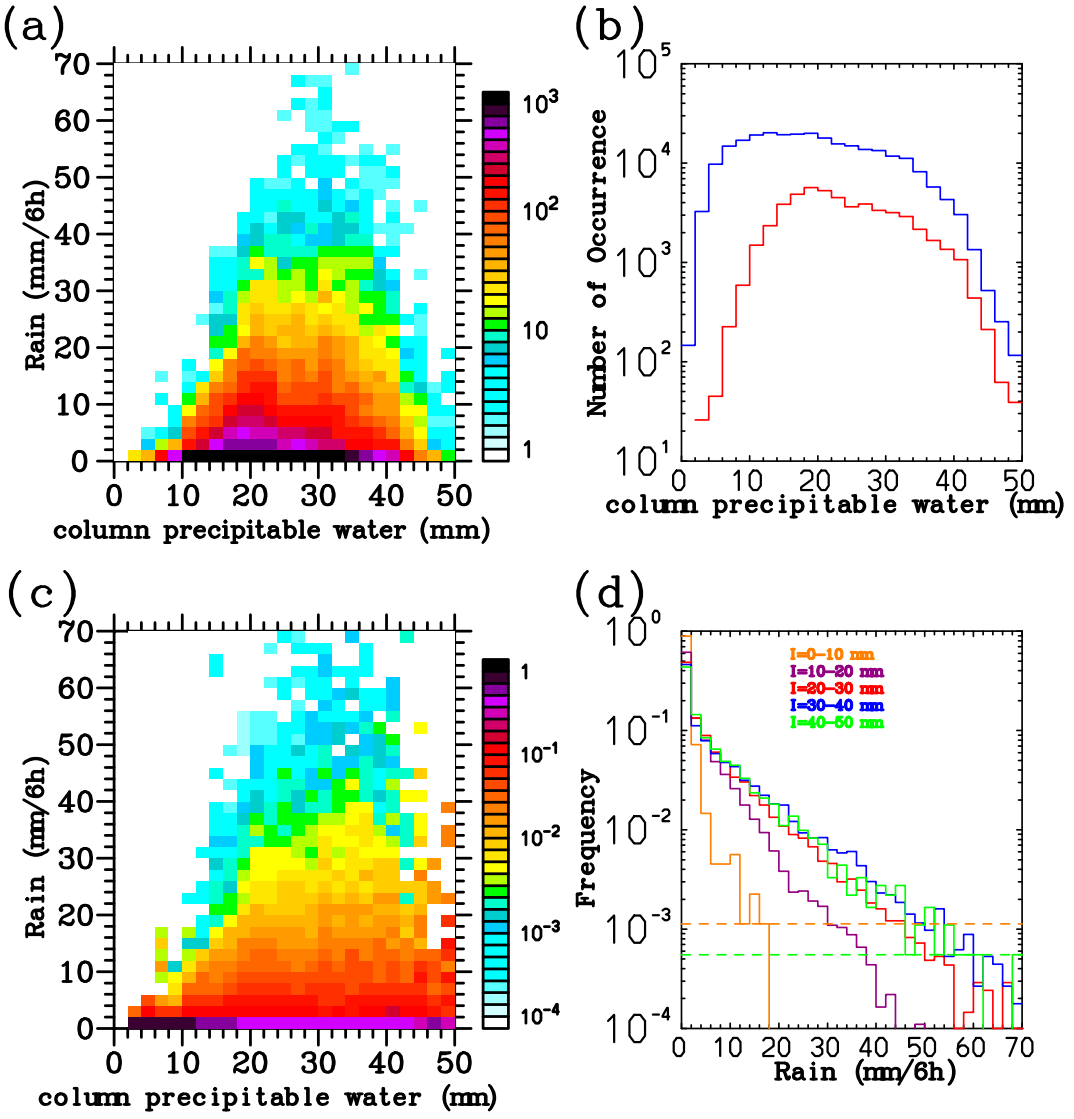

FIG. 8. Statistics during the rain states: (a) joint frequency distribution $p(I, R|R > 0)$ of CPW (mm) and rain [mm (6 h)$^{-1}$]. The number of occurrences is shown for every bin with a size of 2 mm × 2 mm (6 h)$^{-1}$. (b) Number of occurrences of CPW for every 2-mm bin, including (blue) and excluding (red) the zero rain measurements. (c) The conditional frequency distribution $p(R|I, R > 0)$ of rain [mm (6 h)$^{-1}$] is shown by a vertical column at each given CPW bin with a size of 2 mm marked by the horizontal axis. (d) As in (c), but for every 10-mm CPW bin, shown as histograms: 0–10 (orange), 10–20 (violet), 20–30 (red), 30–40 (blue), and 40–50 mm (green). In (d), the values less than 10^{-4} are treated as missing values, indicated by discontinuities in histograms. Also shown in (d) by short-dashed horizontal lines are the minimum possible frequencies due to finite numbers of cases available (i.e., sample size).

the expected rain intensity $\overline{R}(R > R_c, I)$ as functions of both the available moisture I and the rain intensity range $R > R_c$ to consider. This question is formally stated in section 3e. Here, we should clearly recognize that chances $P(R > R_c|I)$ for rain under a given large-scale moisture state I are clearly different depending on the magnitudes of rains in concern, as conditioned by $R > R_c$ with the threshold R_c. Less obviously, the expected intensity of rain $\overline{R}(R > R_c, I)$ also changes with the magnitude of rains in concern as well.

The main nobility of the present study is, thus, to examine the rain statistics systematically varying the rain intensity threshold. As it turns out, the characteristics of the rain statistics sensibly depend on a range of the rain intensity considered. In the infinitesimal regime [$R_c < 1$ mm (6 h)$^{-1}$], a common expectation that both the rain probability and the expected intensity increase with the increasing available moisture in the atmosphere (Fig. 4) is confirmed. However, recall that there could be also substantial errors with the lowest rain measurements (cf. section 3).

A qualitatively different picture emerges when finite rains with $R_c \geq 1$ mm $(6\ \text{h})^{-1}$ are considered. The frequency (probability) of occurrence of rain also increases with increasing available moistures I in the finite regime [$R_c \geq 1$ mm $(6\ \text{h})^{-1}$: Fig. 5a]. However, the expected rain intensity (Fig. 5b), increases only weakly with increasing CPWs with the rain thresholds $R_c \geq 1$ mm $(6\ \text{h})^{-1}$ and in a less pronounced manner than for the frequency of occurrence (cf. Figs. 5c,d). A separate analysis in the appendix further suggests that those weak dependencies on CPW are overall within the data uncertainties.

The obtained result is rather in odd with a common notion of attributing a high moisture state as a *cause* of extreme rain events and floods. Here, analysis is rather subtle: our statistical analyses have been performed under rain conditions. With the statistics including the non-rain state, a different picture emerges: the average rain, indeed, increases with increasing available moistures, as shown in Fig. 3. Many studies e.g., Waliser and Guan (2017) perform the analyses from this different perspective.

However, the present study points out something more: the average rain increases with increasing moistures mostly because of an increasing chance of rain. This conclusion is qualitatively consistent with a finding of Powell (2019) that an area average rain increases by overall following increasing fractional rain areas, if the area average and the fractional area can be conceptually re–interpreted as temporal average and probability, respectively. This further suggests that long-distance transport of moisture, for example, by atmospheric rivers may contribute in enhancing a chance of rain, but an ultimate cause of extreme events should be sought in something else.

Nevertheless, it is important to keep in mind that these major findings of the present study apply only for the finite rains with $R_c \geq 1$ mm $(6\ \text{h})^{-1}$. A more commonly expected rain behavior is recovered in the infinitesimal regime with $R_c < 1$ mm $(6\ \text{h})^{-1}$. This sensitive threshold dependence of rain behavior is another important aspect elucidated by the present study.

As suggested in section 3, the transition of regimes from infinitesimal to finite can be understood in analogy with the transition from linear to nonlinear regimes in hydrodynamic instabilities (Drazin and Reid 1981): this transition occurs at a relatively small threshold, 1 mm $(6\ \text{h})^{-1}$. According to categorization of drizzle by both WMO (Annex, https://library.wmo.int/doc_num.php?explnum_id=3160) and the AMS Glossary (American Meteorological Society 2020), 1 mm in 6 h corresponds to drizzle rather than any significant rain. Thus, any reasonable amount of rains (i.e., those not categorized as drizzle) falls into the finite regime, and the rather unintuitive tendency identified in this study follows. However, the identified threshold, 1 mm $(6\ \text{h})^{-1}$, is hardly a sharp transition point, but the transition occurs only gradually over this threshold, as seen in Fig. 5, somehow corresponding to the transition from drizzle to rain in conventional categorizations.

The most important reminder from the present study is basic: rain is not a simple, straight consequence of conversion of available moisture. A rain forms only as a consequence of certain a dynamical mechanism, for example, by a frontogenesis associated with a low pressure cyclone as seen in weather maps (cf. Shapiro and Grønås 1999), or alternatively, by a much local convective instability (Doswell 2001; Houze 2014), or more generally, by a combination of both (Markowski and Richardson 2010), maybe also assisted by the presence of mountains (Rotunno and Houze 2007). To induce an extreme rain, a given atmospheric column does not need to contain all the water required to fall, say, in the next 6 h: atmospheric flows can supply more moisture required, and the aforementioned dynamical mechanisms can provide means for generating and maintaining such a state by positive feedback processes.

Finally, it may be remarked that the present study is only based on an analysis over a particular region of the globe. For a good demonstration, the present study has chosen one of the most rain intense areas in Central Europe (Friuli Venezia Giulia, northeast Italy: Manzato 2007; Feudale and Manzato 2014; Isotta et al. 2014; Manzato et al. 2016, 2019; Poelman et al. 2016; Pavan et al. 2019). Nevertheless, some of the details of the results could be specific to the chosen region. For this reason, more extensive observational analyses would still be required to verify a generality of the present result, especially a tendency for constancy of the expected rain intensity with increasing available moisture in the atmosphere.

Acknowledgments. Ian Jolliffe, Victor Homar, Ileana Blade, and Marcello Miglietta critically commented on earlier drafts. We also thank the four anonymous reviewers and editor-in-charge, Susan van den Heever, helping us to finalize the manuscript. Figure 1 is prepared by Andrea Cicogna at OSMER-ARPA FVG.

APPENDIX

Data Uncertainties

In interpreting the results with the averages and the frequencies evaluated from data, certain details come into question. For example, in Fig. 3a, we find a sharp negative peak at 44 mm followed by a sharp positive peak at 46 mm for both full years and convective seasons: is this an artifact due to a limited number of cases available in data, and will a different result be found for a different period? Only if these possibilities are excluded, these behaviors can be accepted as *universal*. These issues can be called *data uncertainties*. This appendix reviews a basic probability theory to estimate data uncertainties, and applies it to the present data analysis.

Suppose a stochastic process that produces a value x. The simplest example is coin tossing: we assign values $+1$ and -1 for the top and the tail, respectively, in this case. Throwing dice is another example. We generalize those examples into stochastic processes that generate values for, say, x, which may either be continuous and discrete. We assume that events (e.g., tossing) are independent to each other, and a chance to take a value x at each event occurs solely based the probability distribution $p(x)$.

We expect that the average value taken by such a process to be simply a *statistical* average (or an expectation value):

$$\bar{x} = \int_{-\infty}^{+\infty} xp(x)dx, \tag{A1}$$

with the actual integral range limited by setting the probability to be zero outside its possible values. However, only in the limit of $n \to \infty$, the actual average value, say, $\bar{x}(n)$, obtained by observing n events becomes identical to the above expectation $\bar{x}$. So long as n is finite, there is always a discrepancy between the measured average $\bar{x}(n)$ and the theoretical expectation $\bar{x}$. In other words, measurements based on a finite number of cases do not provide a true average. That is an essence of the data uncertainties.

The law of large numbers (cf. Ch. X, Feller 1968) states that the root-mean-square error $\left\langle [\bar{x}(n) - \bar{x}]^2 \right\rangle^{1/2}$ of the estimate follows:

$$\left\langle [\bar{x}(n) - \bar{x}]^2 \right\rangle^{1/2} = \beta\sigma/n^{1/2}, \tag{A2}$$

when n is large enough. Here, σ is the standard deviation *of distribuition* obtained from the probability distribution $p(x)$, and β is a constant that is independent of number n of events. It follows that, generally, data uncertainty may be estimated by

$$\left\langle [\bar{x}(n) - \bar{x}]^2 \right\rangle^{1/2} \sim \sigma/n^{1/2}, \tag{A3}$$

by order of magnitude. The right-hand side of Eq. (A3) is called the standard error of the mean. It states that the uncertainty of the average estimate $\bar{x}(n)$ is bounded by the spread in the distribution of x, as measured by the standard deviation σ and decreases with the increasing number n of measurements by the factor of $n^{-1/2}$. The theory outlined here provides a basis of many statistical significance tests available in literature with an exact value of β depending on the form of $p(x)$ (cf. Wonnacott and Wonnacott 1969; Gregory 2005).

Keep in mind that the estimate (A3) of the uncertainty is obtained by assuming that the value x is generated by a random, independent sequence of events. On the other hand, a natural process such as rain, as considered herein, is hardly a random process, but a result of a deterministically defined natural law. Thus, the theory developed here is not directly applicable to natural processes.

A usual approach to amend this problem is to assume that a given time series is still defined by a type of *quasi-random* process (cf. Zwiers and von Storch 1995, section. 6.6.7 in von Storch and Zwiers 1999): i.e., although n measurements may not be totally independent to each other, a given time series can be interpreted to be equivalent to a process with $n^*(<n)$ random measurements. This number n^* is called the degrees of freedom (Jenkins and Watts 1968), or alternatively the equivalent sampling size (von Storch and Zwiers 1999), the effective data size (Mudelsee 2010). Thus, Eq. (A3) is revised into

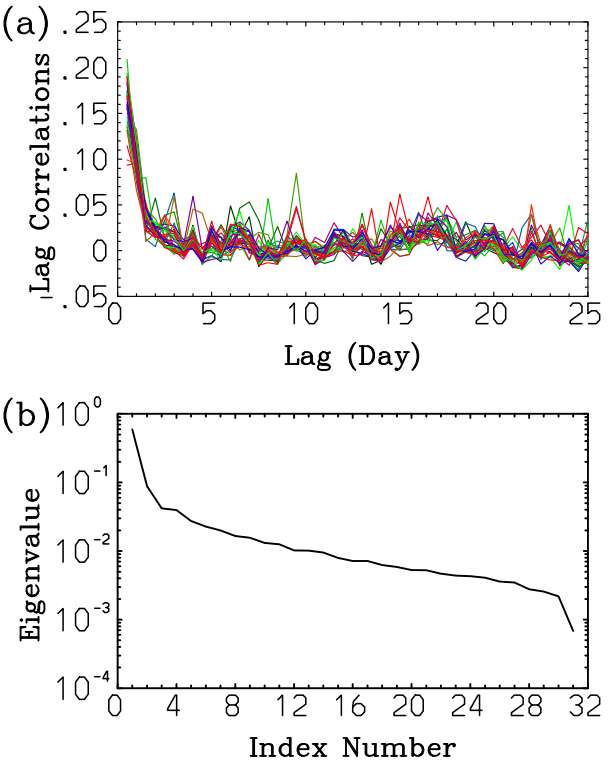

FIG. A1. Analysis for estimating the degrees of freedom n^* of data. (a) Auto-lag correlations of 33 individual station time series, plotted with varying colors of curves. (b) Fractional contributions of SVD vectors to explain the total variance of data.

$$\left\langle [\bar{x}(n) - \bar{x}]^2 \right\rangle^{1/2} \sim \sigma/n^{*1/2}. \tag{A4}$$

Although there is an inherent ambiguity in determining such a number n^*, we follow standard procedures (cf. Zwiers and von Storch 1995, section 7.1 in von Storch and Zwiers 1999). The present rain dataset consists of a time series of rain gauge measurements by 33 stations. Thus, there are dependencies both in time and space (i.e., mutual dependence between the stations), and the degrees of freedom must be defined for both dependencies.

The degrees of freedom in time are estimated from auto-lag correlations of time series of the 33 rain gauge stations (Fig. A1a). From these lag-correlation plots, we estimate a characteristic lag time to be $\tau = 2$ days, based on the fact that beyond this time scale, the correlations simply remain fluctuated over the range of 0–0.05 like a background noise. Thus, we divide the number of measurements by $\tau/0.5(\text{day}) = 4$ to obtain an estimate of the temporal degree of freedom, i.e., the degrees of freedom of data in time are a quarter (1/4) of the total number of measurements in time.

To estimate a spatial degree of freedom of the 33 stations, a singular vector decomposition (SVD: Hannachi et al. 2007) is applied to the covariances between these 33 station measurements. The obtained singular values (eigenvalues) measure fractional contributions of singular vectors to the total

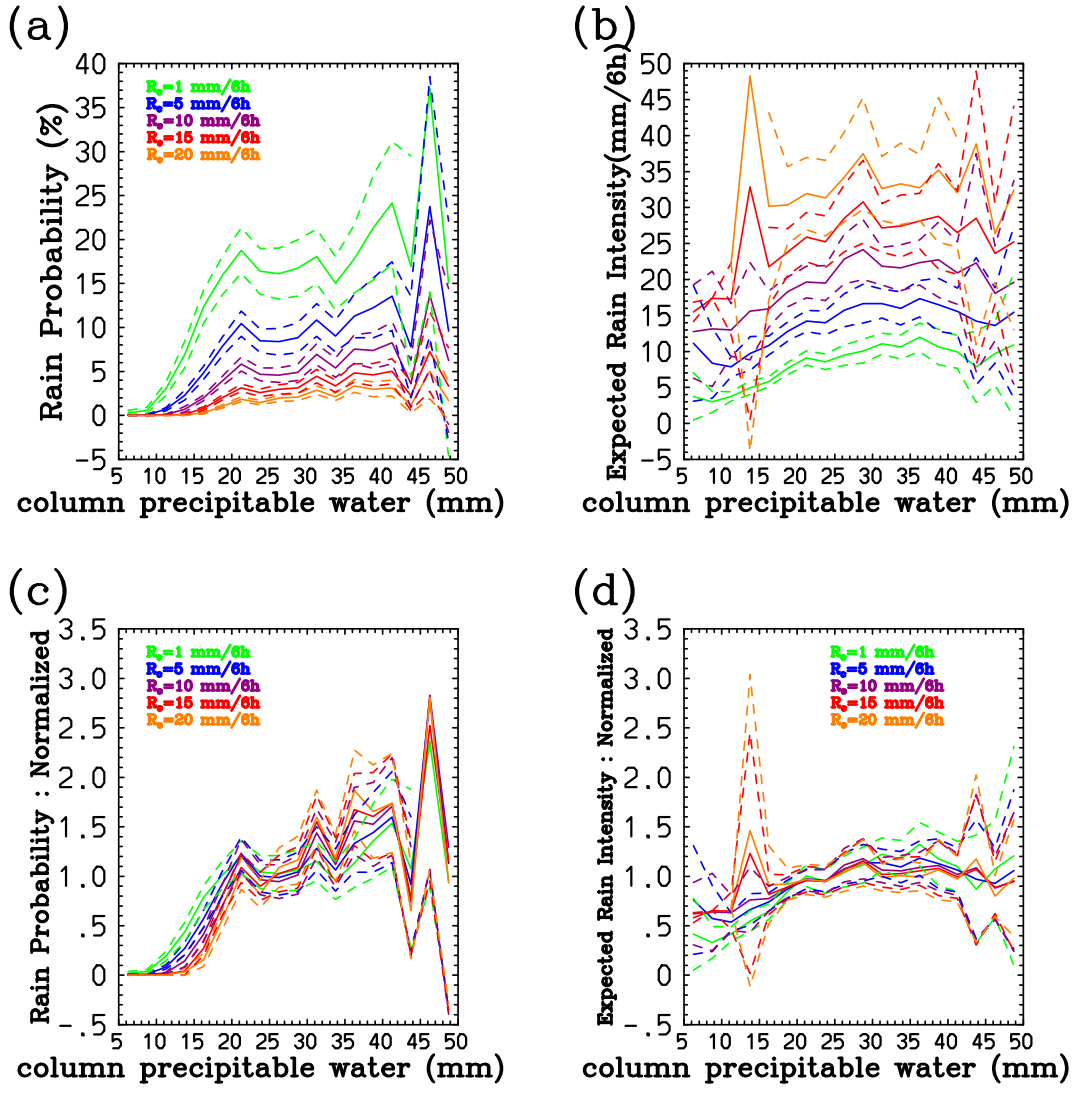

FIG. A2. The same solid curves are as in Fig. 5, but mark the uncertainties by short-dashed curves. Extreme uncertainty values are omitted from the plot.

variability Fig. A1b). An estimate of degrees of freedom can conceptually proceed in analogous manner as in North et al. (1982), but here in a much more qualitative manner: the rain time series of those 33 rain gauge stations are all positively correlated with the minimum covariance 0.32 obtained between the stations 3 and 32 of Table 1. For this reason, the covariance matrix also turns out to be rather singular, and a pair of eigenvectors is degenerated, presumably due to two stations closely located to each other. As a result, only the 31 singular values are obtained. The first vector explains about 60% of the total variance, and the explained fractional variance overall decreasing exponentially with increasing index numbers. By adding those contributions together, the first three vectors explain 73% of the total variance, the first 10 88%, and the explained variance increases only more gradually by further increasing numbers of singular vectors. Based on these observations, we judge the degree of freedom with the 33-station measurements to be about three, i.e., the spatial degree of freedom of data is about 1/10 of the total number of rain gauge stations.

By combining those results both in time and space, we conclude that the degrees of freedom are about 1/4 × 1/10 = 1/40 of the number of measurements, i.e., $n^* = n/40$. Here, n is the number data available for every given subset, for example, per CPW bin and as conditioned by the rain threshold. A standard deviation σ is also evaluated from the given n subset of measurements. The upper and lower bounds of uncertainties are then evaluated based on in Eq. (A4) by adding $\pm\sigma/n^{*1/2}$ to the average, and plotted, for example, by short-dashed curves in Fig. 3. Uncertainty analyses for Figs. 5b and 5d are shown in Figs. A2b and A2d, respectively, in the same manner.

Unfortunately, the uncertainties associated with the frequencies (probabilities) cannot be estimated in a similar

manner: we do not have any information on the distribution of probability, in the same sense as for physical variables. Instead, we estimate the probability uncertainties in two alternative manners.

The first is simply to use the minimum frequency $1/n$ resolved by data with the number of cases n as marked by short-dashed horizontal lines in Fig. 8d: given data cannot measure any smaller frequencies than this value.

The second is to invoke the principle of the propagation of errors (Hallett 2003): from Eq. (10), we find that the errors $\delta^*\overline{R}(I)$ and $\delta^*\overline{R}(R>R_c,I)$ in $\overline{R}(I)$ and $\overline{R}(R>R_c,I)$ propagate to the probability error $\delta^*P(R>R_c|I)$ by

$$\frac{\delta^*P(R>R_c|I)}{P(R>R_c|I)} \simeq \frac{\delta^*\overline{R}(R>R_c,I)}{\overline{R}(R>R_c,I)} - \frac{\delta^*\overline{R}(I)}{\overline{R}(I)}.$$

Note the two errors tend to cancel each other in defining the probability error. However, in practice, even the relative signs of those two errors are unknown. Thus, we adopt the following rule:

$$\frac{\delta P(R>R_c|I)}{P(R>R_c|I)} = \max\left[\frac{\delta\overline{R}(R>R_c,I)}{\overline{R}(R>R_c,I)}, \frac{\delta\overline{R}(I)}{\overline{R}(I)}\right] \tag{A5}$$

for estimating the probability uncertainty $\delta P(R>R_c|I)$ from the uncertainties $\delta R(I)$ and $\delta\overline{R}(R>R_c,I)$ of $R(I)$ and $\overline{R}(R>R_c,I)$, respectively. The obtained probability uncertainties are plotted by short-dashed curves in Figs. A2a and A2c.

REFERENCES

Ahmed, F., and C. Schumacher, 2015: Convective and stratiform components of the precipitation-moisture relationship. *Geophys. Res. Lett.*, **42**, 10 453–10 462, https://doi.org/10.1002/2015GL066957.

American Meteorological Society, 2020: "Drizzle." Glossary of Meteorology, https://glossary.ametsoc.org/wiki/Drizzle.

Bertó, A., A. Buzzi, and D. Zardi, 2004: Back-tracking water vapour contributing to a precipitation even over Trentino: A case study. *Meteor. Z.*, **13**, 189–200, https://doi.org/10.1127/0941-2948/2004/0013-0189.

Besson, L., 1924: On the probability of rain. *Mon. Wea. Rev.*, **52**, 308–308, https://doi.org/10.1175/1520-0493(1924)52<308a:OTPOR>2.0.CO;2.

Buzzi, A., S. Davolio, P. Malguzzi, O. Drofa, and D. Mastrangelo, 2014: Heavy rainfall episodes over Liguria in autumn 2011: Numerical forecasting experiments. *Nat. Hazards Earth Syst. Sci.*, **14**, 1325–1340, https://doi.org/10.5194/nhess-14-1325-2014.

Cavanaugh, N. R., A. Gershunov, A. K. Panorska, and T. J. Kozubowski, 2015: The probability distribution of intense daily precipitation. *Geophys. Res. Lett.*, **42**, 1560–1567, https://doi.org/10.1002/2015GL063238.

De Zolt, S., P. Lionello, A. Nuhu, and A. Tomasin, 2006: The disastrous storm of 4 November 1966 on Italy. *Nat. Hazards Earth Syst. Sci.*, **6**, 861–879, https://doi.org/10.5194/nhess-6-861-2006.

Dingman, S. L., 1994: *Physical Hydrology.* 2nd ed. Prentice Hall, 646 pp.

Doswell, C. A., III, Ed., 2001: *Severe Convective Storms. Meteor. Monogr.*, No. 50, Amer. Meteor. Soc., 561 pp.

Drazin, P. G., and W. H. Reid, 1981: *Hydrodynamic Stability.* Cambridge University Press, 527 pp.

Epstein, E. S., 1966: Point and area precipitation probabilities. *Mon. Wea. Rev.*, **94**, 595–598, https://doi.org/10.1175/1520-0493(1966)094<0595:PAAPP>2.3.CO;2.

Feller, W., 1968: *An Introduction to Probability Theory and Its Applications.* 3rd ed. Vol. 1. John Wiley and Sons, 509 pp.

Feudale, L., and A. Manzato, 2014: Cloud-to-ground lightning distribution and its relationship with orography and anthropogenic emissions in the Po valley. *J. Appl. Meteor. Climatol.*, **53**, 2651–2670, https://doi.org/10.1175/JAMC-D-14-0037.1.

Grazzini, F., G. C. Craig, C. Keil, G. Antolini, and V. Pavan, 2020: Extreme precipitation events over northern Italy. Part I: A systematic classification with machine-learning techniques. *Quart. J. Roy. Meteor. Soc.*, **146**, 69–85, https://doi.org/10.1002/qj.3635.

Gregory, P., 2005: *Bayesian Logical Data Analysis for the Physical Sciences.* Cambridge University Press, 468 pp.

Hallett, J., 2003: Measurement in the atmosphere. *Handbook of Weather, Climate, and Water: Dynamics, Climate, Physical Meteorology, Weather Systems, and Measurements*, T. D. Potter and B. R. Colman, Eds., Wiley Interscience, 711–720, https://doi.org/10.1002/0471721603.ch35.

Hammarstrand, U., 1980: A model to predict the probability of precipitation. *Mon. Wea. Rev.*, **108**, 793–803, https://doi.org/10.1175/1520-0493(1980)108<0793:AMTPTP>2.0.CO;2.

Hannachi, A., I. T. Jolliffe, and D. B. Stephenson, 2007: Empirical orthogonal functions and related techniques in atmospheric science: A review. *Int. J. Climatol.*, **27**, 1119–1152, https://doi.org/10.1002/joc.1499.

Houze, R., Jr., 2014: *Cloud Dynamics.* 2nd ed. Academic Press, 432 pp.

Isotta, F. A., and Coauthors, 2014: The climate of daily precipitation in the Alps: Development and analysis of a high-resolution grid dataset from pan-Alpine rain-gauge data. *Int. J. Climatol.*, **34**, 1657–1675, https://doi.org/10.1002/joc.3794.

Jenkins, G. M., and D. G. Watts, 1968: *Spectral Analysis and Its Applications.* Holden–Day, 525 pp.

Jorgensen, D. L., 1968: Note on the combining of two probabilities by means of a scatter diagram. *Mon. Wea. Rev.*, **96**, 887–888, https://doi.org/10.1175/1520-0493(1968)096<0887:NOTCOT>2.0.CO;2.

Kalnay, E., 2002: *Atmospheric Modeling, Data Assimilation and Predictability.* Cambridge University Press, 368 pp.

Khain, A. P., and M. Pinsky, 2018: *Physical Processes in Clouds and Cloud Modeling.* Cambridge University Press, 626 pp.

Khodayar, S., N. Kalthoff, and C. Kottmeier, 2018: Atmospheric conditions associated with heavy precipitation events in comparison to seasonal means in the western Mediterranean region. *Climate Dyn.*, **51**, 951–967, https://doi.org/10.1007/s00382-016-3058-y.

Krichak, S. O., P. Alpert, and M. Dayan, 2004: The role of atmospheric processes associated with Hurricane Olga in the December 2001 floods in Israel. *J. Hydrometeor.*, **5**, 1259–1270, https://doi.org/10.1175/JHM-399.1.

——, ——, and ——, 2006: An evaluation of the role of Hurricane Olga (2001) in an extreme rainy event in Israel using dynamic tropopause map. *Meteor. Atmos. Phys.*, **98**, 35–53, https://doi.org/10.1007/s00703-006-0230-7.

——, J. Barken, J. S. Breitgang, S. Gualdi, and S. B. Feldstein, 2015: The role of the export of tropical moisture into

midlatitudes for extreme precipitation events in the Mediterranean region. *Theor. Appl. Climatol.*, **121**, 499–515, https://doi.org/10.1007/s00704-014-1244-6.

Kuo, Y.-H., J. D. Neelin, and C. R. Mechoso, 2017: Tropical convective transition statistics and causality in the water vapor–precipitation relation. *J. Atmos. Sci.*, **74**, 915–931, https://doi.org/10.1175/JAS-D-16-0182.1.

Lavers, D. A., and G. Villarini, 2013: The nexus between atmospheric rivers and extreme precipitation across Europe. *Geophys. Res. Lett.*, **40**, 3259–3264, https://doi.org/10.1002/grl.50636.

——, R. P. Allan, E. F. Wood, G. Villarini, D. J. Brayshaw, and A. J. Wade, 2011: Winter floods in Britain are connected to atmospheric rivers. *Geophys. Res. Lett.*, **38**, L23803, https://doi.org/10.1029/2011GL049783.

Leonard, A., 1975: Energy cascade in large-eddy simulations of turbulent flows. *Advances in Geophysics*, Vol. 18A, Academic Press, 237–248, https://doi.org/10.1016/S0065-2687(08)60464-1.

Lilly, D. K., 1967: The representation of small-scale turbulence in numerical simulation experiments. *Proc. IBM Scientific Computing Symp. on Environmental Sciences*, Yorktown Heights, NY, IBM, 195–210.

Malguzzi, P., G. Grossi, A. Buzzi, R. Ranzi, and R. Buzzia, 2006: The 1966 "century" flood in Italy: A meteorological and hydrological revisitation. *J. Geophys. Res.*, **111**, D24106, https://doi.org/10.1029/2006JD007111.

Manzato, A., 2005: The use of sounding-derived indices for a neural network short-term thunderstorm forecast. *Wea. Forecasting*, **20**, 896–917, https://doi.org/10.1175/WAF898.1.

——, 2007: The 6 h climatology of thunderstorms and rainfalls in the Friuli Venezia Giulia Plain. *Atmos. Res.*, **83**, 336–348, https://doi.org/10.1016/j.atmosres.2005.08.013.

——, A. Cicogna, and A. Pucillo, 2016: 6-hour maximum rain in Friuli Venezia Giulia: Climatology and ECMWF-based forecasts. *Atmos. Res.*, **169B**, 465–484, https://doi.org/10.1016/j.atmosres.2015.07.013.

——, A. Pucillo, and A. Cicogna, 2019: Improving ECMWF-based 6-hour maximum rain using instability indices and neural network. *Atmos. Res.*, **217**, 184–197, https://doi.org/10.1016/j.atmosres.2018.10.020.

Mapes, B. E., E. S. Chung, W. M. Hannah, H. Masunaga, A. J. Wimmers, and C. S. Velden, 2018: The meandering margin of the meteorological moist tropics. *Geophys. Res. Lett.*, **45**, 1177–1184, https://doi.org/10.1002/2017GL076440.

Markowski, P., and Y. Richardson, 2010: *Mesoscale Meteorology in Midlatitudes.* Wiley-Blackwell, 407 pp.

Miloshevich, L. M., H. Vömel, D. N. Whiteman, and T. Leblanc, 2009: Accuracy assessment and correction of Vaisala RS92 radiosonde water vapor measurements. *J. Geophys. Res.*, **114**, D11305, https://doi.org/10.1029/2008JD011565.

Mudelsee, M., 2010: *Climate Time Series Analysis.* Springer, 474 pp.

Neelin, J. D., O. Peters, and K. Hales, 2009: The transition to strong convection. *J. Atmos. Sci.*, **66**, 2367–2384, https://doi.org/10.1175/2009JAS2962.1.

North, G. R., T. L. Bell, R. F. Cahalan, and F. J. Moeng, 1982: Sampling errors in the estimation of empirical orthogonal functions. *Mon. Wea. Rev.*, **110**, 699–706, https://doi.org/10.1175/1520-0493(1982)110<0699:SEITEO>2.0.CO;2.

Pavan, V., and Coauthors, 2019: High resolution climate precipitation analysis for north-central Italy, 1961–2015. *Climate Dyn.*, **52**, 3435–3453, https://doi.org/10.1007/s00382-018-4337-6.

Poelman, D. R., W. Schulz, G. Diendorfer, and M. Bernardi, 2016: The European lightning location system EUCLID—Part 2: Observations. *Nat. Hazards Earth Syst. Sci.*, **16**, 607–616, https://doi.org/10.5194/nhess-16-607-2016.

Pop, S. B., 2000: *Turbulent Flows.* Cambridge University Press, 771 pp.

Powell, S. W., 2019: Observing possible thermodynamic control on tropical marine rainfall in moist environments. *J. Atmos. Sci.*, **76**, 3737–3751, https://doi.org/10.1175/JAS-D-19-0144.1.

Pruppacher, H. R., and J. D. Klett, 1997: *Microphysics of Clouds and Precipitation.* 2nd ed. Kluwer Academic Publishers, 954 pp.

Ralph, F. M., T. Coleman, P. J. Neimn, R. J. Zamora, and M. D. Dettinger, 2013: Observed impacts of duration and seasonality of atmospheric-river landfalls on soil moisture and runoff in coastal Northern California. *J. Hydrometeor.*, **14**, 443–459, https://doi.org/10.1175/JHM-D-12-076.1.

Reynolds, W. C., 1990: The potential and limitations of direct and large eddy simulations. *Whither Turbulence? Turbulence at the Crossroads*, J. L. Lumly, Ed., Springer-Verlag, 313–343.

Rotunno, R., and R. A. Houze, 2007: Lessons on orographic precipitation from the Mesoscale Alpine Programme. *Quart. J. Roy. Meteor. Soc.*, **133**, 811–830, https://doi.org/10.1002/qj.67.

Schaefer, J. T., and R. L. Livingston, 1990: Operational implications of the "probability of precipitation." *Wea. Forecasting*, **5**, 354–356, https://doi.org/10.1175/1520-0434(1990)005<0354:OIOTOP>2.0.CO;2.

Schiro, K. A., J. D. Neelin, D. K. Adams, and B. R. Lintner, 2016: Deep convection and column water vapor over tropical land versus tropical ocean: A comparison between the Amazon and the tropical western Pacific. *J. Atmos. Sci.*, **73**, 4043–4063, https://doi.org/10.1175/JAS-D-16-0119.1.

Shapiro, M. A., and S. Grønås, Eds., 1999: *The Life Cycles of Extratropical Cyclones.* Amer. Meteor. Soc., 412 pp.

Siccardi, F., 1996: Rainstorm hazards and related disasters in North-West Mediterranean region. *Remote Sens. Rev.*, **14**, 5–21, https://doi.org/10.1080/02757259609532311.

Sorí, R., R. Nieto, A. Drumond, M. Stojanovic, and L. Gimeno, 2019: On the connection between atmospheric moisture transport and dry conditions in rainfall climatological zones of the Niger River Basin. *Water*, **11**, 622, https://doi.org/10.3390/w11030622.

Trenberth, K. E., 1998: Atmospheric moisture residence times and cycling: Implications for rainfall rates and climate change. *Climatic Change*, **39**, 667–694, https://doi.org/10.1023/A:1005319109110.

Vaisala, 2013: Vaisala radiosonde RS92 performance in the WMO intercomparison of high quality radiosonde systems. Vaisala, 17 pp., https://www.vaisala.com/sites/default/files/documents/WEA-MET-WMO-Test-White_Paper-B211129EN-D-LOW.pdf.

Vömel, H., and Coauthors, 2007: Radiation dry bias of the Vaisala RS92 humidity sensor. *J. Atmos. Oceanic Technol.*, **24**, 953–963, https://doi.org/10.1175/JTECH2019.1.

von Storch, H., and F. W. Zwiers, 1999: *Statistical Analysis in Climate Research.* Cambridge University Press, 484 pp.

Waliser, D., and B. Guan, 2017: Extreme winds and precipitation during landfall of atmospheric rivers. *Nat. Geosci.*, **10**, 179–183, https://doi.org/10.1038/ngeo2894.

Wonnacott, T. H., and R. J. Wonnacott, 1969: *Introductory Statistics.* John Wiley and Sons, 402 pp.

Yano, J.-I., 2015: Scale separation. *Parameterization of Atmospheric Convection*, R. S. Plant and J. I. Yano, Eds., Vol. I, World Scientific, Imperial College Press, 73–99.

——, and ——, 2012: Convective quasi-equilibrium. *Rev. Geophys.*, **50**, RG4004, https://doi.org/10.1029/2011RG000378.

——, M. Bister, Z. Fuchs, L. Gerard, V. Phillips, S. Barkidija, and J. M. Piriou, 2013: Phenomenology of convection-parameterization closure. *Atmos. Phys. Chem.*, **13**, 4111–4131, https://doi.org/10.5194/acp-13-4111-2013.

——, and Coauthors, 2014: Basic concepts for convection parameterization in weather forecast and climate models: COST action ES0905 final report. *Atmosphere*, **6**, 88–147, https://doi.org/10.3390/atmos6010088.

——, M. H. P. Ambaum, H. Dacre, and A. Manzato, 2020: A dynamical–system description of precipitation over the tropics and the midlatitudes. *Tellus*, **72**, 1–17, https://doi.org/10.1080/16000870.2020.1847939.

Zhu, Y., and R. E. Newell, 1994: Atmospheric rivers and bombs. *Geophys. Res. Lett.*, **21**, 1999–2002, https://doi.org/10.1029/94GL01710.

Zwiers, F. W., and H. von Storch, 1995: Taking serial correlation into account in tests of the mean. *J. Climate*, **8**, 336–351, https://doi.org/10.1175/1520-0442(1995)008<0336:TSCIAI>2.0.CO;2.